4-6-2010

Design of a Galvanic Vestibular Stimulation based Collision Avoidance System for the Visually Impaired

Paul Quevedo
McMaster University

Recommended Citation

Quevedo, Paul, "Design of a Galvanic Vestibular Stimulation based Collision Avoidance System for the Visually Impaired" (2010). *EE 4BI6 Electrical Engineering Biomedical Capstones.* Paper 58.
http://digitalcommons.mcmaster.ca/ee4bi6/58

Design of a Galvanic Vestibular Stimulation based Collision Avoidance System for the Visually Impaired

by

Paul Quevedo

Electrical and Biomedical Engineering
Faculty Advisor: Prof. T. Doyle

Electrical and Biomedical Engineering Project Report
submitted in partial fulfillment of the degree of
Bachelor of Engineering

McMaster University
Hamilton, Ontario, Canada
April 6, 2010

ABSTRACT

To date many different attempts at assisting the visually impaired navigate busy environments have been explored. Most systems use an array of sensors to map the environment around the subject and by use of auditory cues or wearable vibrators, indicate which direction the subject should move in to avoid a collision. This report outlines the design of a system to use Galvanic Vestibular Stimulation as another modality to manoeuvre subjects from a collision course.

Bipolar Galvanic Vestibular Stimulation (GVS) entails the use of a low frequency, low amplitude current, typically 1mA, passed between the mastoid processes of a person causing a sensation of imbalance towards the anodal electrode. It is an already established method of altering a person's balance and has been found to affect the trajectory of a person walking in a given direction.

The design of the system is a network of microcontrollers in which a control unit collects data from sensors, builds a map of the environment, determines the optimal direction to proceed and controls the current stimulator to deliver the desired GVS. Using the Controller Area Network (CAN) protocol allows for a highly modular system design in which any type of sensor or data node can easily be added or removed from the system.

The system was prototyped and tested. Initial results indicate the system is capable of navigating a person from a trajectory course however several issues are encountered in quantifying the systems effectiveness. All subsystems performed as desired however certain ones were found to be over engineered for the task required. The results of the systems performance are discussed and areas for improvement highlighted.

ACKNOWLEDGEMENTS

TABLE OF CONTENTS

LIST OF FIGURES

LIST OF TABLES

INTRODUCTION

1.1 BACKGROUND

The work in this report pertains to the design of a collision avoidance system to aid the visually impaired in navigating an environment. A person with a visual impairment would typically employ the use of a white cane or guide dog to assist them in these situations. A white cane is a simple light weight cane used to detect objects a short distance ahead of the user. They're range however is very limited and hence can only provide a limited information to the user about the environment around them. Guide dogs on the other hand are able to accurately navigate complex and dynamic environments with great success. They do however, require special training, constant care and can be quite expensive. Such a solution is not always practical then.

Recently there have been systems developed by research groups that use vibration and acoustic feedback cues to indicate to the user which direction to move in to avoid obstacles [1,2]. These systems employ ultrasonic transducers to map the environment around the user then through use of a microprocessor, determine what direction cues the system should give to the use. Such systems have proven to be successful as collision avoidance tools for the visually impaired and it the focus of this report to build on those concepts using a different type of feedback mechanism.

Bipolar Galvanic Vestibular Stimulation (GVS) is the process by which a small amount of current is passed between the mastoid processes of a standing subject in order to stimulate the nerves in the vestibular system. Doing so causes an involuntary lateral sway in a subject towards to the anodal stimulating electrode [4]. When applied to a subject while walking this stimulation causes a deviation in trajectory [5,6]. It is the goal of this report then to employ vestibular stimulation as the main user feedback mechanism of a collision avoidance system and investigate whether it can successfully navigate a visually impaired person through a dynamic environment.

1.2 OBJECTIVES AND PROJECT SCOPE

The primary goal of this project is to combine the Galvanic Vestibular Stimulation technique with a collision avoidance system and investigate its abilities to navigate a person through an environment.

The design of the system is intended to be very modular and unrestrictive on the sensors that can be used to map the environment. The system should only be concerned with the spatial data of objects in the environment and not how they are acquired. This allows for a designer implementing this system to choose the best sensors to suit their needs as well as an easy way to make updates or improvements.

Since sensor selection and design is not in the scope of this project a method of evaluating the systems functionality must be devised. This method must also allow for evaluation of the primary objective of this project stated in the beginning of this section.

The system needs to evaluate the best trajectory around the objects it is aware of and thus an effective collision avoidance algorithm needs to be developed. This algorithm needs to have the least amount of computational complexity possible allowing for execution on inexpensive platforms.

This project will encompass the development of all hardware and software required to implement the system. No range finding sensors will be developed but details on how to interface a sensor module to the system will be provided.

In order to validate the systems functionality, a virtual sensor will be devised to provide pre-programmed information for the system to process. Test scenarios will be created based on the information programmed into the virtual sensor and the effect of the system examined.

LITERATURE REVIEW

2.1 COLLISION AVOIDANCE SYSTEMS

Current systems for collision avoidance are comprised of three main elements: sensor array for object detection and localization, user feedback mechanism for trajectory correction and a controller to determine said trajectory. The systems developed by Shin et al [2] and Cardin et al

[1] employ the use of ultrasonic transceivers as the sensors used for object detection. These rangefinders are small, easy to use and relatively inexpensive. They do however have some limitations. They're technology is based on timing how long a reflected sound wave takes to reach the sensor. If a sound wave does not hit an object at a perpendicular angle, a large amount of the reflected sound energy is lost and the sensor may not be able to detect that object [3]. The material composition of different objects also plays a role in reducing the reflected sound energy. Other problems arise in the sensors field of view, FOV. Ultrasonic sensors emit sound waves in a cone that diverges with distance. As an example the HX40TR ultrasonic sensor by Hexamite has a beam width of ±12 degrees. Localizing objects then at further distances can become difficult with such sensors. As a result of the shortcomings of these ultrasonic transceivers, sensor selection and design was left out of the scope of this project.

The user feedback for trajectory correction in the systems by Shin et al and Cardin et al both use vibration motors placed in the shoulders of a jacket or vest. To indicate a left or right course direction the appropriate motor is simply turned on for a brief period of time. In addition to this the system by Shin et al uses auditory cues in conjunction with vibration to better indicate directions to the user. This system is implemented using an ARM9 based embedded system which for the minimal amount of computation seems overly expensive in terms of cost. The system developed by Cardin et al uses an 8-bit microcontroller, a more cost effective platform.

The system by Cardin et al claims a 50% reduction in time required for navigating around obstacles with a bit of prior training. The system by Shin et al doesn't quantify their results however they claim to be able to effectively navigate a corridor with a dead end and objects scattered throughout.

2.2 COLLISION AVOIDANCE ALGORITHMS

In the systems described in section 2.1 the algorithms used for collision avoidance were based on a known number and configuration of sensors. Look up tables for different combinations of sensor information are used to determine the situation and course of action for the system by Shin et al. This project however is supposed to be impartial to the choice and configuration of sensors used in the system. A different type of algorithm will be needed then.

In robotics a commonly used algorithm for real-time collision avoidance is the Nearness Diagram (ND) technique developed by Minguez et al [7,8]. This method takes a 360 degree mapping of the environment surrounding the robot and extracts information on the spatial location of all objects in order to determine the motion commands. Two maps are created in this method. The first called a PND (Nearness Diagram from the Central Point), searches for gaps between objects that the robot can navigate through to reach a set goal point. The second is called a RND (Nearness Diagram from the Robot) evaluates if any objects are too close to the robot. Based on the features of these two maps a robot is placed into different safety situations which affects the criteria and calculations for the robots desired trajectory.

The exact calculations used in this technique however, are not of significant importance to this project since GVS does not provide a high level of control as is possible with robots. The PND map is the main concept that will be carried forward in this project. It is sufficient to determine whether the best gap between objects to proceed in is left or right of the subjects' current position.

2.3   GALVANIC VESTIBULAR STIMULATION

Bipolar Galvanic Vestibular Stimulation is the process by which a small amount of current is passed between the mastoid processes of a standing subject in order to stimulate the nerves in the vestibular system. It has been shown that when low amplitude currents (0.5 - 1mA) are applied at low frequencies (~0.5-2Hz) involuntary mediolateral sway is induced in a standing subject in which they sway towards the anodal stimulating electrode [4,9]. The effects of GVS are most pronounced in the absence of any visual sensory information. A minimum current is required in order for stimulation to have any effect and is referred to as the threshold current. This threshold current is a minimum around 0.75 to 1Hz with a value less than 1mA [10]. Threshold values do vary from person to person.

Additional studies have looked at the effect of bipolar GVS on subjects while walking in the absence of visual information and have found a relationship between the amplitude of the current applied and the magnitude of deviation in the subjects walking trajectory [5,6]. Mixed results between these studies indicate some uncertainty in whether a subject can sense their deviation from the intended path. Some subjects appear to be aware of their deviation and correct

for it once the applied current stimulus is removed while others remain unaware and continue on along the new trajectory.

The work by Fitzpatrick et al indicates that the walking trajectory of the subject does not change until the second step after stimulation with maximum change at step 3 [6]. This suggested latency in stimulation response needs to be taken into consideration in the design of this project. Cadence of the subject also plays a role in how much effect GVS has while walking. Slower cadences require more reliance on the vestibular system for balance and thus the effects of GVS are more pronounced [6].

Additionally it has been shown that subjects do not necessarily have a symmetric minimum threshold response to GVS between their left and right sides. The magnitude effect of GVS past threshold also does not have a symmetric response between left and right sides on any given subject [5].

The works reviewed in this section pertaining to GVS often use constant or low frequency current stimulation. In the case of low frequency stimulation no mention is made to whether the applied pulses are biphasic and therefore it assumed that all stimulation used results in charge build up in the tissue. The system will then follow suite and not use any biphasic pulses to deliver GVS. This limits electrode selection to metal electrodes which will not depolarize over time.

2.4   ELECTRODE TISSUE INTERFACE

Since controlled currents will be delivered through the brain using external electrodes, an understanding is required of how the electrode tissue interface behaves as well as safety limitations placed on the maximum current densities allowed. Currently there no set limits on the maximum safe current density that can be used without damage to the skin and tissues for transcranial stimulation. An article published in the journal of Clinical Neurophysiology suggests that a current density of 25.46 A/m^2 can be applied for 20 minutes without skin damage and minimal sensation [11]. Assuming 1cm diameter electrodes and 3mA stimulation the current density is less than 1 A/m^2 suggesting safe use for prolonged periods of time.

A review of electric currents applied to skin cites the limit for tolerable skin sensation at a current density of 0.5mA/cm^2 [12]. An empirically derived formula for the maximum painless current is also cited in this work as:

$$I = \frac{28.6A}{48.3+A} \qquad (1)$$

where I is the current in mA and A is the electrical contact area in cm^2. Using this formula with 1cm diameter electrodes indicates that the maximum current for painless stimulation is 0.455 mA. Considering that threshold current for GVS is between 0.5 to 1.0 mA it is expected that some minor discomfort will be encountered during stimulation. This formula is derived from empirical data and therefore the amount of discomfort is expected to vary from person to person.

In comparing the findings of this paper with the suggestions of the previously mentioned work it is assumed that since the maximum intended current density of this project is well under 25.46 A/m^2 but large enough that some sensation and possibly discomfort may be felt it will still be kept to a minimal value.

Looking now at the electrical impedance of the tissue electrode interface, the tissue/skin interface is typically modelled as an RC network shown in Figure 1 [13].
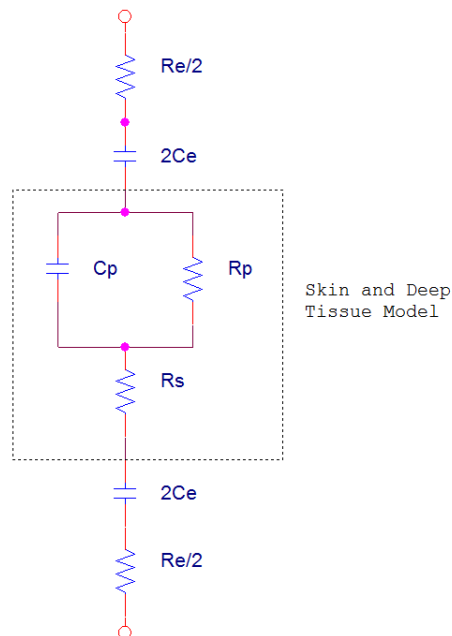
Figure 1: Electrical model of Tissue-Electrode interface. Rp and Cp model the skin with Rs modelling bulk tissue. Electrode-electrolyte interface are represented by Re and Ce

From the model it is apparent that the Rp Cp parallel combination imposes a frequency dependence on the skin's impedance. The work by Lykken [14] however found that removal of

the most superficial layer of skin, the stratum corneum, effectively removes this parallel Rp Cp impedance thus removing any frequency dependence. The work by Boxtel [13] shows that removal of the stratum corneum results in significant reduction in the magnitude of the skins impedance as indicated in Figure 2.
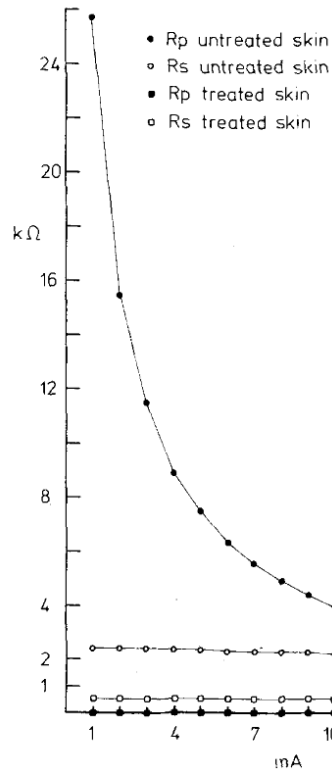
Figure 2: "Relation between the current intensity (instantaneous current at the end of the pulse) and skin resistance components Rp and Rs when square voltage pulses were applied to intact skin or to skin with the stratum corneum removed." Figure and description from the work published by Boxtel 1977 [13]

The effective impedance of the skin tissue interface can vary in magnitude depending on frequency, skin treatment, electrode type and whether any conductive gels are used. Conductive gels help reduce the impedance between electrode and tissue and are commonly used whenever attaching electrodes to skin. In the worst case scenario where gel is applied to the electrode skin interface but the skin is untreated the effective impedance at 1Hz can be anywhere between 10kΩ to 1MOhm [15]. In the case of treated skin and use of an electrode gel, the effective impedance of a 1.8cm diameter gold electrode using Ten-20 gel and treated skin is modelled and measured to be as good as 8kΩ at 30Hz stimulation [16]. It's therefore presumed that the impedance of the tissue electrode interface will be greater than 8kΩ at 1Hz stimulation and less than 100kΩ in the worst case where skin is not treated properly.

DESIGN METHODOLOGY

3.1 COLLISION AVOIDANCE SUBSYSTEM

The project is divided in two main subsystems. The first subsystem revolves around data acquisition and processing required for collision avoidance.

The Nearness Diagram method outlined in section 2.2 is the foundation for the algorithm developed in this project. This algorithm is chosen as it can be adapted to be impartial to the configuration and field of view of the sensors used. It has the benefit of being a highly accurate algorithm intended for use in dynamic environments. It provides precise trajectories for robots to follow however since GVS cannot provide this level of control in directing a person the algorithms do not need to be as complex. This allows for simplification in its implementation in terms of computational power required. The collision avoidance algorithm will be implemented on an 8-bit microcontroller that acts as the Master Control Unit (MCU) of the system. An 8bit microcontroller provides enough computing power, memory and onboard peripherals necessary for this system.

The location of the objects reported are kept track of by the MCU and as such the subjects orientation relative to these objects needs to be maintained. A magnetometer can be used as a compass to keep track of the persons heading. This also allows for slower update rates of the sensors to the MCU resulting in less network traffic. In addition to the magnetometer the system also needs to be keep track of when a person is walking. The system should only stimulate to alter a subject's trajectory and thus stimulation of a stationary subject needs to be avoided. Measuring a person's walking speed is difficult and unnecessary for this system. A pedometer should provide sufficient information on whether a subject is walking or stationary. The combination of these two sensors makes up the Trajectory Measurement Unit (TMU) of the system.

3.2 VESTIBULAR STIMULATION SUBSYSTEM

The systems second main subsystem is the stimulation unit. The impedance of the electrode tissue interface is expected to be larger than the ideal case of 8kΩ. In the worst case scenarios where skin is not properly treated prior to electrode attachment the impedance can reach 1MOhm. Delivering a current at this impedance requires dangerously high voltages and as such the system will be limited to delivering a maximum of 3mA at 30kΩ impedance. As a result the necessary voltages required to achieve this is ±90V. This high level of voltage is not available from typical batteries and hence a bipolar power supply will be needed to create the necessary high voltages from two +9 volt batteries.

In general there are ways of stepping up a DC voltage. One method is to convert the DC signal to an AC one and use a center tapped transformer to create the necessary positive and negative voltages. The two voltages can then be rectified and buffered. Center tapped transformer coil can however be quite expensive and provide no flexibility in adjusting the power and voltages outputted. If for example, it is found during the design stage that ±90V is too high for safe use of this system then a new transformer coil would have to be purchased.

An alternate method is to use a switching mode power supply. These supplies use fast switching transistors, inductors and capacitors to boost DC voltages with very high efficiency. They are generally controlled using microchips or timing circuits. Using a microchip to control the switching of the transistors allows for design flexibility in the power and voltage outputs. Implementation only requires capacitors, inductors and some discrete components meaning it's fairly inexpensive. Changes to the power output are also easily made by simply reprogramming the microchip. This method will be used to implement the power supply.

The stimulation unit needs to provide a constant current over a range of varying impedances. The simplest solution is then to use a high voltage op-amp to implement a bipolar current source.

3.3   MICROCONTROLLER NETWORK

The microcontroller network provides a way for sensors to be easily added and interfaced to the existing system. The network bus needs to be robust, cheap, widely available and provide a simple method of adding nodes. The Controller Area Network (CAN) bus provides all of these features. It is multi-master network that provides error detection and speeds up to 1Mbps. It uses a 2 wire differential bus for serial communication between nodes providing such features as message prioritization, filtering, multicast reception and configuration flexibility. The configuration flexibility means that any node can be added to the network by simply splicing the 2 wire bus to connect to the new node.

Implementation is achieved by using a CAN controller and a CAN transceiver to interface to the bus. The controller, commonly found on most microcontrollers today but can also be realized as a separate IC, generates and processes messages on the CAN bus. The transceivers job is to convert the single ended signals to and from the controller to a differential signal to be sent over the bus. These components are relatively inexpensive meaning the network is cheap to implement. A complete description of the CAN protocol and physical layer is available in the specification document by Bosch [18].

3.4   SYSTEM OVERVIEW

A block diagram of the system showing how each subsystem connects to each other is shown in Figure 3. The stimulation subsystem is controlled entirely by the MCU. The MCU is responsible for enabling and disable the high voltage supply as well as generating the stimulation waveform by use of an on-chip digital to analog (DAC) converter.
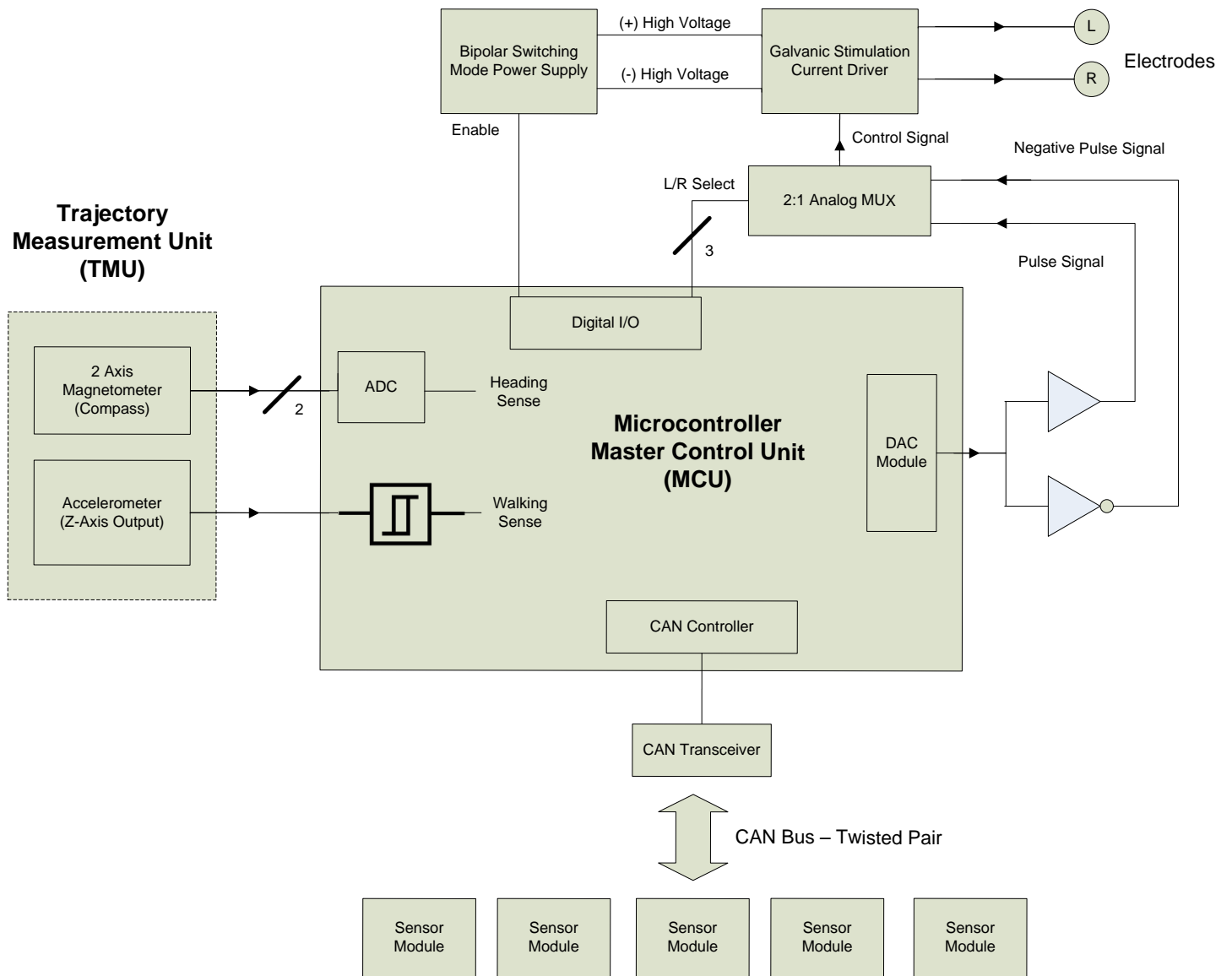
Figure 3: Block diagram showing how the different subsystems connect

SYSTEM DESIGN: HARDWARE

This section outlines in detail the hardware design of each part of the system. Circuit diagrams, design justifications and component selections are presented.

4.1 STIMULATION CURRENT SOURCE

Stimulation of the vestibular system must be done using a voltage controller current source. The exact impedance of the skin tissue interface is not known and will also fluctuate with time as moisture builds on the skin. Vestibular stimulation requires delivery of a fixed current value alternating at about a 1Hz rate. A simple current source circuit is shown in Figure 4.
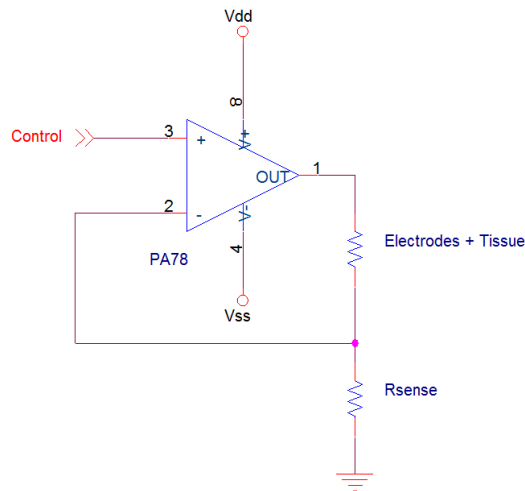
Figure 4: Schematic for simple bipolar current source

The voltage at the V+ terminal must match the voltage at the V- terminal which is the measured voltage drop over the R_{sense} resistor. By controlling the voltage at the V+ terminal this circuit will control the amount of current passing through both the electrodes and the sense resistor such that the voltage drop over R_{sense} matches the control voltage.

From the literary research done on the tissue electrode interface it is known that its impedance can be at best 8kΩ or potentially exceeding 100kΩ depending on the skin preparation. The electrodes chosen to deliver the GVS will be 1cm diameter gold plated cup electrodes commonly used in EEGs. These reusable electrodes are metal and will not depolarize when using monophasic pulses. The impedance of the tissue electrode interface was assumed to

be 30kΩs in the worst case. A maximum of 3mA stimulation is desired and as such supply rails for the op-amp shown in Figure 4 must then be ±90V. Using rails of ±100V will compensate for any voltage loss in the op-amp.

Most operational amplifiers are not suited to handle these high voltages. The PA78 power amplifier from Cirrus Logic was chosen for this circuit because of its high supply rails (±10 – 175V) and modest quiescent current draw (0.7mA typical). The value of R_{sense} is chosen to be 1kΩ so that the voltage of the control signal equates to the current in mill amperes passed through the electrodes.

The control signal is a square wave generated by the microcontroller based MCU using the on-chip voltage reference module as a DAC to control the amplitude. The signal is at a frequency of 0.5952Hz generated by using the microcontrollers' timer to module. More information about the generation of this signal is present in section 5.4 . The microcontroller is however only able to generate a signal with amplitude greater than 0V. In order to achieve bipolar stimulation an inverter is used to invert the control signal and an analog multiplexor to select between the positive and negative wave. The schematic of this setup is shown in Figure 5.
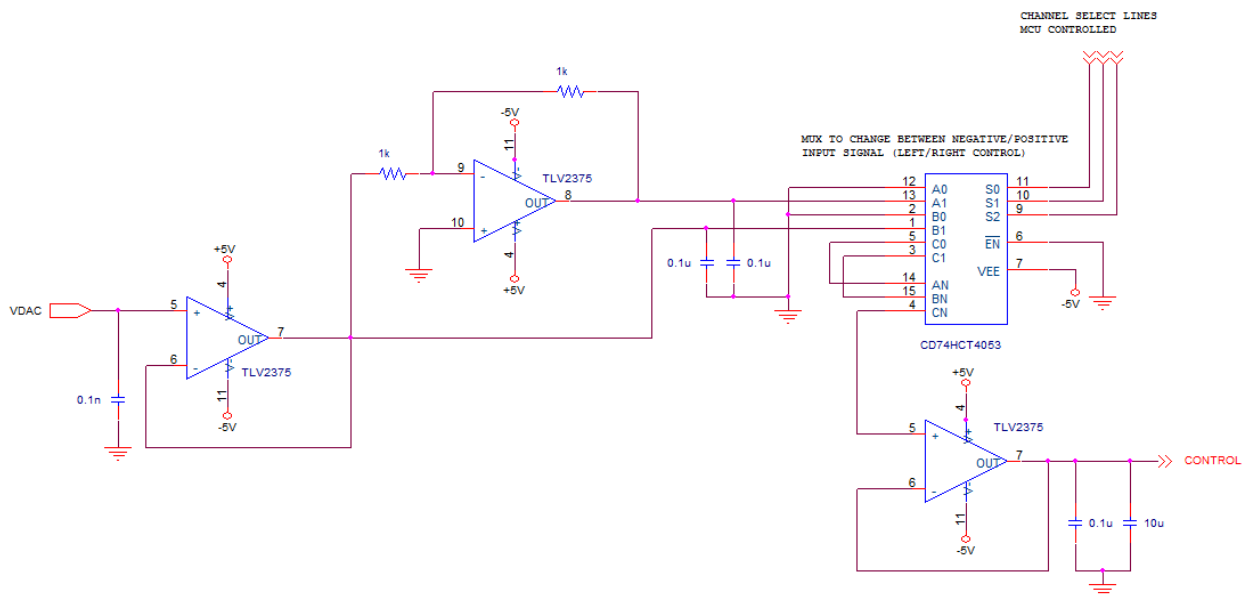
Figure 5: Multiplexing of the control signal generated by the microcontroller, VDAC.

The CD74HCT4053 by Texas Instruments contains 3 2:1 multiplexors controlled by three logic select lines. The MCU generates the signal VDAC which is buffered and inverted by the TLV2375 dual supply rail to rail op-amp, also by Texas Instruments. The signals are fed into the multiplexor which outputs the positive signal, negative signal or ground as the control. The

control signal has two bypass capacitors after being buffered and going to the input of the PA78 op-amp. What was found during testing of the circuits is that the switching mode supply and current source board had very large amounts of noise present due to the high voltage and fast switching. If the input of the PA78 is linked directly to the output of the multiplexor the switching noise bleeds into the rest of the circuitry. Using a buffer and high and low value bypass capacitor helps shunt most of this noise.

The complete circuit is shown in Figure 6. Note extra components used with the PA78 op-amp. The 5k resistor in series with a 0.1n capacitor forms a compensator network to limit slew rate of the device. Since the signal is at such a low frequency these components have little effect of the performance of the circuit. The $1k\Omega$ resistor R_{lim} is required by the op-amp to limit the current outputted should a short circuit failure occur. Very low amounts of current are required in this circuit so a relatively high value can be used. No information is given on how to select values for R_{lim} greater than 100Ω (which ensures currents of less than 40mA for supply voltages less than 200V) but through simulation and experimentation with the op-amp a value of $1k\Omega$ was found to work. It can only be inferred that the current limit will be less than 40mA from the graphs provided in the datasheets but without damaging the actual component it is unknown what this limit will be.

A secondary op-amp is shown in place of the PA78. The OPA445 is a precision high voltage op-amp from Texas Instruments supporting supply rails up to ±45V. Justification for its use in place of the PA78 was made during the testing and validation phase of the project. This is discussed in more detail in section 6.2 .
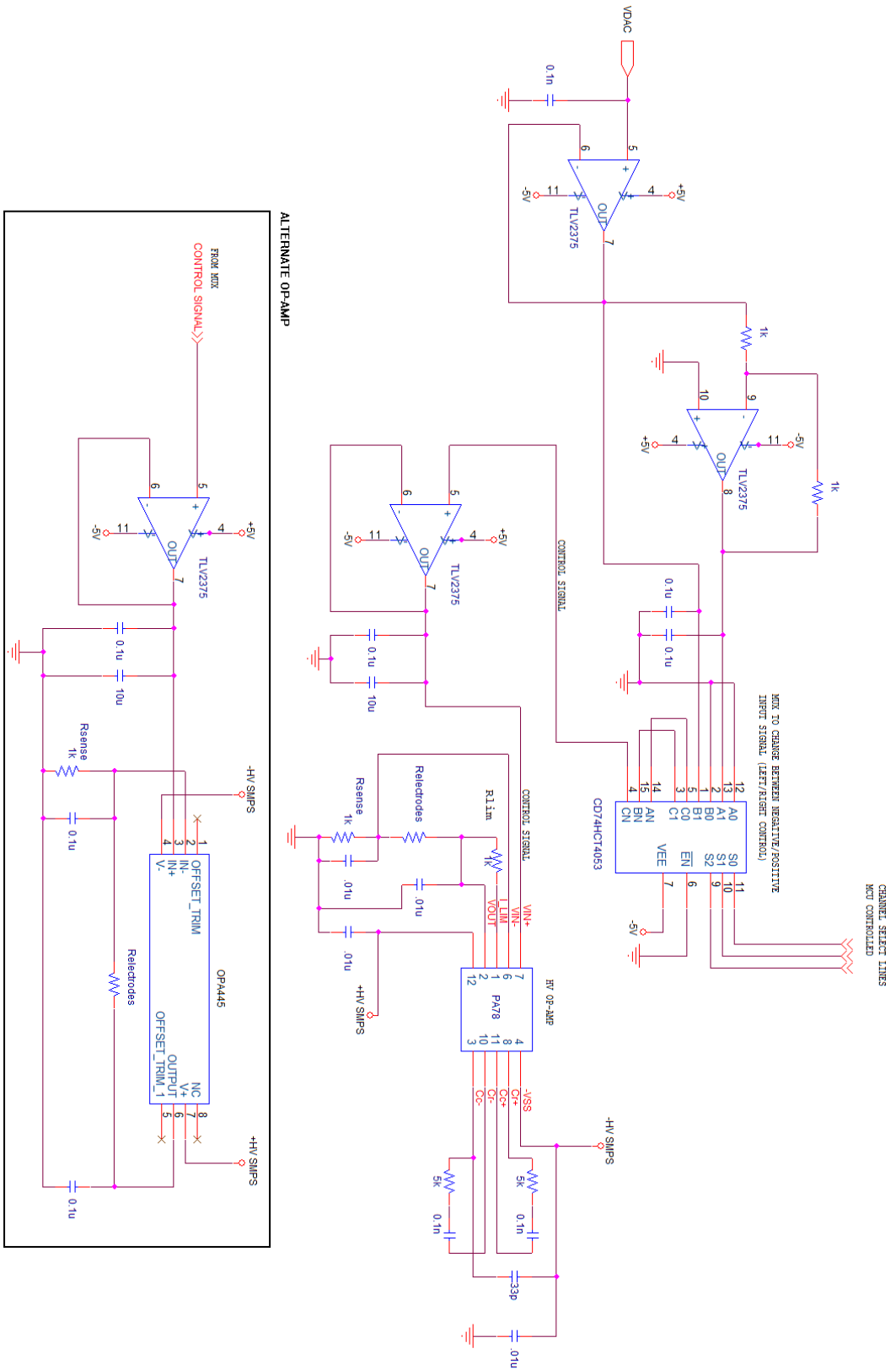
Figure 6: Schematic for the Voltage Controlled Current Source to deliver Galvanic Vestibular Stimulation

4.2 STIMULATION POWER SUPPLY

To provide the necessary ±100V required to power the current source from a battery supply, a bipolar switching mode supply will be used. One of the simplest ways to realize this is using a buck-boost and inverting buck-boost topology shown in Figure 7.
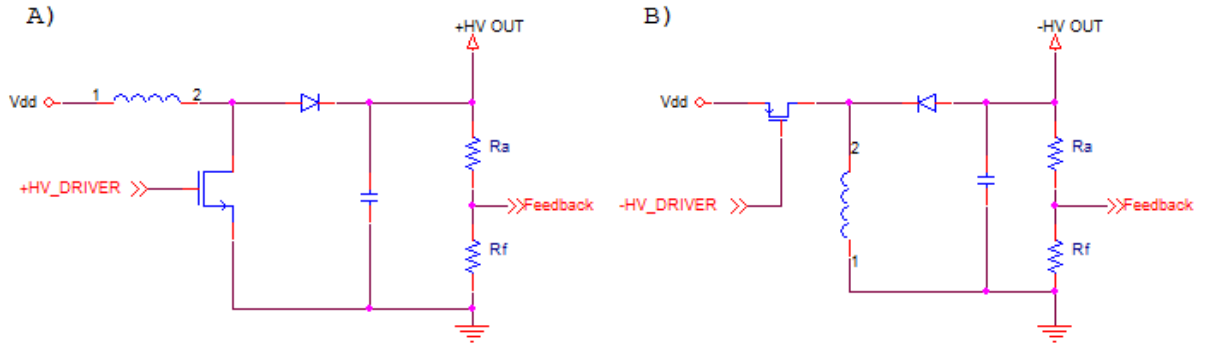
Figure 7: A) Buck-Boost topology and B) Inverting Buck-Boost Topology

The MOSFETs are switched on and off to control the current passed through the inductors. When the FETs are on current builds up linearly on the inductors with time according to the relation $V = L\frac{dI}{dt}$. When off the energy stored in the inductor is discharged over the capacitor which stores the charge from the previous cycle. With each cycle, charge builds up and the magnitude of the voltage increases.

The switching of the FETs will be controlled using a microcontroller so as to allow for easy changes to the timing values during design and testing. Technical bulleting TB053 from Microchip Technology Inc. [19] and the book Switching Power Supply Design [24] were used to aid in the design of this circuit. The references provide the necessary background and equations to calculate the timing of the pulses and the resulting power output of the supply. Starting from the equation for the peak current draw over the inductor a value for the inductor can be chosen.

$$Ipeak = \frac{Vin}{L} * DT \qquad\qquad (2)$$

For Vin = 10V and a peak current draw of less than 500mA so as not to drain the battery excessively fast, a value of 220µH for L equates to a DT value of 10µSec. D is the duty cycle as

of the switching period T. The switching of the FETs will be managed by a microcontroller and as such 10µSec is a reasonable value. The peak current for this value is 455mA.

The duty cycle for the switching signal D, should be about 75% of the period in order to ensure discontinuous operation. Discontinuous operation means that all of the current stored on in the inductor is discharged onto the capacitor before the next pulse cycle. This simplifies design and ensures the inductor does not exceed its maximum intended current draw. If the rise time of the current through the inductor (DT) is 10µSec T should then be 13.2µSec giving a duty cycle D, of 75.76%. The circuit is thus in discontinuous mode for 3.2µSec. The time required by an ideal inductor to discharge entirely is found from the following equation:

$$0 = \frac{Vin - Vout}{L} t_{fall} + I_{peak} \qquad (3)$$

The value of t_{fall} is then 1.12µSec, less than half of the total allocated time of 3.2µSec. The circuit should remain in discontinuous mode at all times then.

The peak power output of the supply is given as:

$$Power = \frac{Vin^2}{2L} * D\text{T} \qquad (4)$$

For Vin = 10V, DT = 10µSec and L = 220µH the peak power is 2.3W. At 100V output the peak current draw from the supply can be 23mA. Assuming max quiescent current draw by the PA78 of 2.5mA and the peak current output onto the electrodes of 3mA at 100V the required power is only 0.55W. In this instance the circuit only needs to be 24% efficient. The peak power is still left at 2.27W because of unknown power losses that would be incurred using prototype breadboards. It is entirely feasible however to reduce the input voltage to less than 10V so that the system could be run off a single 9V battery and still meet the power requirements. By increasing the switching frequency of the FETS the peak power could also be reduced resulting in longer battery life. Battery life however, is not of significant concern at this stage in the design.

In order to regulate the output voltage to 100V the feedback resistors R_f and R_a shown in Figure 7 divide the output voltage which is evaluated by the microcontroller. A comparator is used to determine if the feedback voltage exceeds the desired value (threshold) and turns off the switching signal to the FETS. When the voltage drops below threshold the switching signal is turned back on. For the negative power supply the output voltage needs to be inverted prior to being sent to the microcontrollers' comparator. A dual supply op-amp can be used to do this.

The values of R_f and R_a are chosen as to minimize the current draw through these resistors during operation. This means most of the generated power is transferred to the load instead of wasted through the feedback network. R_a is selected to be 500kΩ and R_f 10kΩ. At 100V the feedback voltage is 1.96V. The internal voltage reference module on the microchip is programmed to be 2V and the comparator simply evaluates if the feedback voltage is less than or greater than this voltage. The switching signal is generated by using the Pulse Width Modulation (PWM) modules on the microcontroller.

The controller is selected as the PIC18F1230 by Microchip Technology which has three comparator inputs and 2 independent PWM modules. The inductors used are 220uH toroidal inductors (model 33221C) from Murata Power Solutions. The inductor has a low effective series resistance (ESR) of 102mΩ, peak current draw of 1.6A and its toroidal shape means the majority of the magnetic field generated is contained inside the inductors core reducing EMI emissions. The capacitors are 7.5uF film capacitors (model FFB24I0755K) with a low ESR of 14mΩ and peak current of 3.1A. The low ESR of film capacitors equates to low amplitude ripples in the supply output. Use of other types of capacitors with poor ESR characteristics will make for a noisy and inefficient power supply. Film capacitors are however quite large but cheaper in price than other low ESR capacitor types, typically hybrid or specially designed electrolytic capacitors. 7.5uF is chosen mainly because of the increased price of higher value capacitors.

The switching transistors are chosen as the FDU3N40 NMOS by Fairchild Semiconductor and IRFU9310 PMOS by Vishay Siliconix. These transistors have high V_{DS} voltages, tolerate up to 1A of current and have fast rise and fall times. The V_{GS} required to turn on these transistors is however 10V which is outside the range of the microcontrollers PWM output. The TC4428A MOSFET driver by Microchip Technology is used to compensate for this. The complete circuit for the power supply is shown in Figure 8. The C code programmed into the PIC18F1230 is included in 7 Appendix D. As a power saving feature the code is only executed when the MCU sets the enable line high.

Take note of the bypass capacitors around the switching transistors. These capacitors are crucial in reducing the ringing noise generated by the transistors. Without them the ringing voltage as the supply reaches the regulated output voltage become significantly large. The pair of 33pF capacitors should be rated for at least 150V and values found through experimentation.
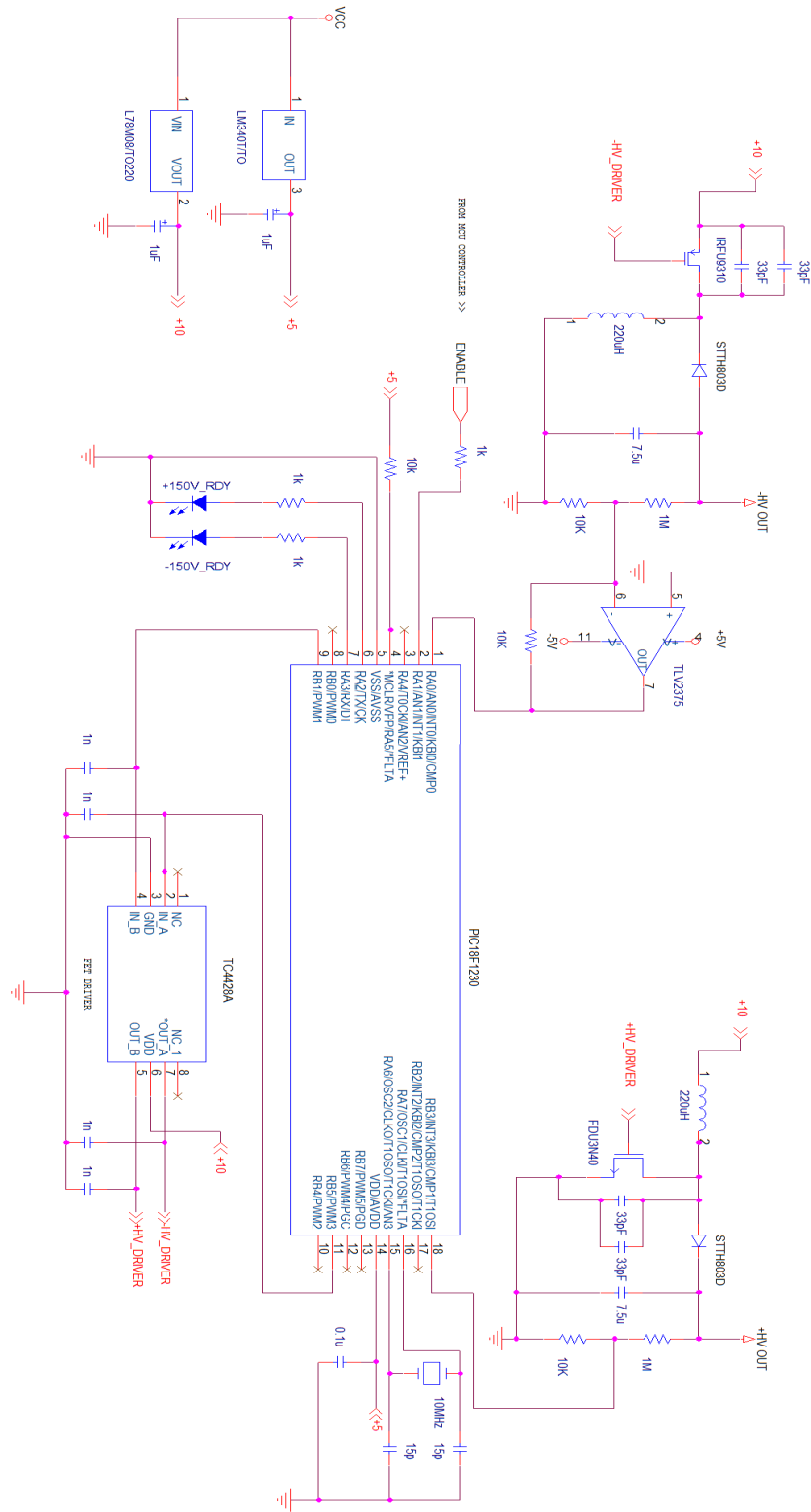
Figure 8: Complete schematic for bipolar 100V switching mode supply.

Care must also be taken in the layout of these components. Originally designed on a solderless breadboard, the high voltage noise generated by the circuit propagated throughout all other circuitry rendering most of it useless. It was transferred to a perfboard and the component arranged so as to minimize the effects of any ground bounce. A good design note on dealing with ground bounce in DC-DC converters can be found in a design article by Analog Devices Jeff Barrow [20]. Essentially the area enclosed by a passing current builds up a magnetic field. When this current is switched of the magnetic field collapses causing a large voltage spike to appear along the entire current path. Since the ground line is part of this path the voltage spike is referred to as ground bounce. Figure 9 illustrates this principal for the inverting buck boost topology.
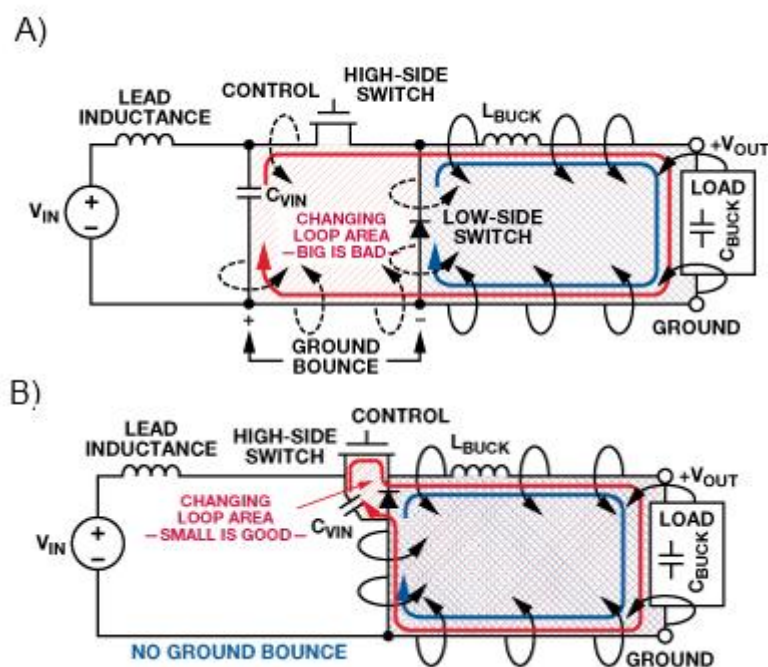
Figure 9: A) Large area where a magnetic field (coming out of the page) is stored. When this field collapses a large voltage is generated along the changing loop area path. B) Minimized changing loop area means less ground bounce. Figures obtained from the ground bounce design article by Jeff Barrows [20].

To minimize the effects of ground bounce the changing loop area should be minimized to be as small as possible. The size of the large components and grid like structure of the perfboard limits just how much this area can be minimized. A picture of the implemented circuit showing the changing loop area for each switching supply is shown in Figure 10.
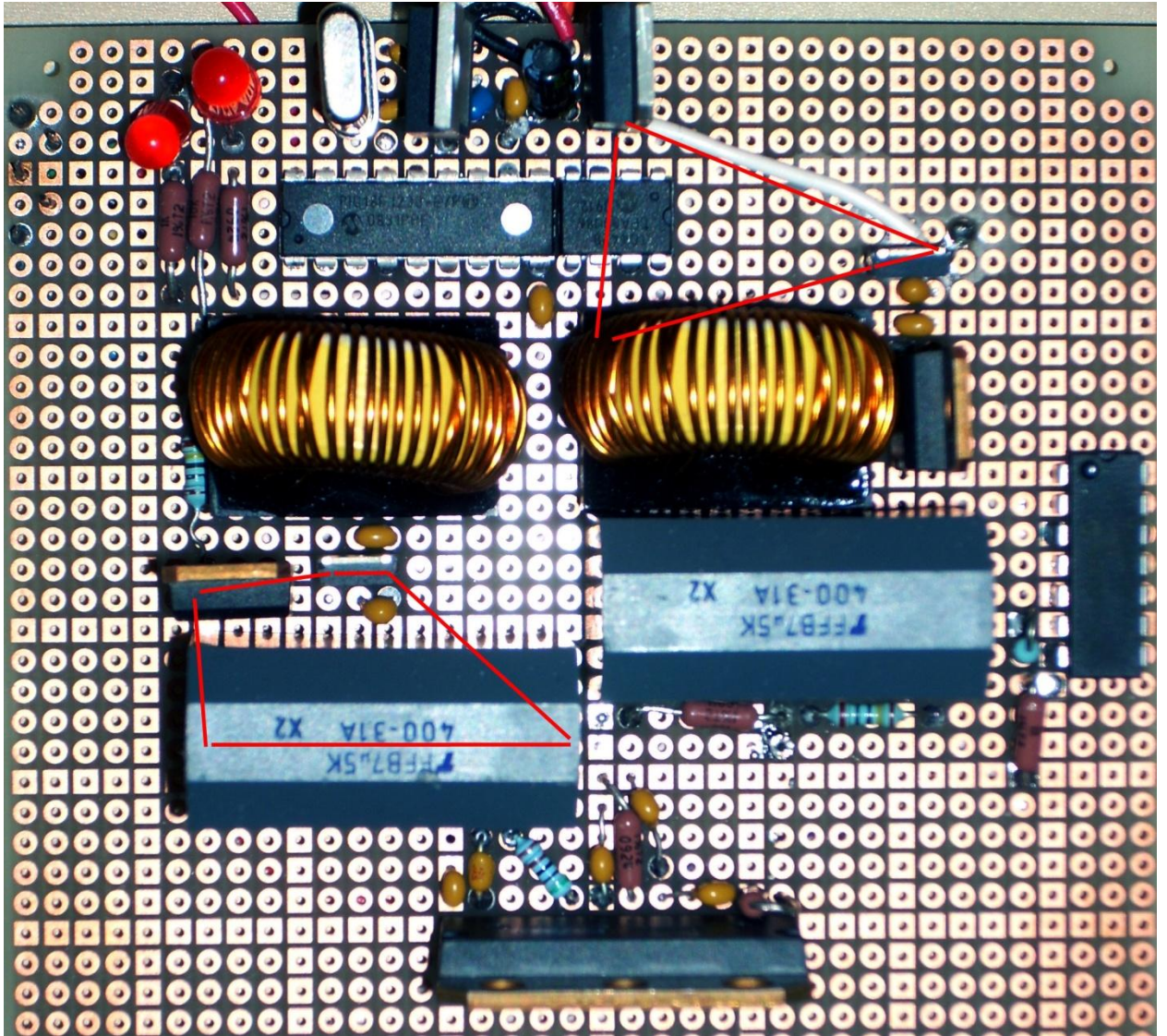
Figure 10: Power Supply Circuit. Red lines indicate the changing loop area that can induce ground bounce

4.3 TRAJECTORY MEASUREMENT UNIT: MAGNETOMETER

The TMU is responsible for determining the heading of a person relative to North and whether they are currently walking or standing stationary. A two axis magnetometer, the HMC1022 by Honeywell International, was used to determine heading. The HMC1022 is a solid state highly sensitive magnetometer capable of detecting fields from 27µgauss to 6 gauss. The sensor is composed of magneto-resistive elements arranged in a Wheatstone bridge. The sensitivity of the sensor is 1mV/V/gauss. For a bridge value of 5V the sensitivity is 5mV/gauss. The earths' field in North America has a maximum value of 0.6gauss [21]. In order to obtain a usable signal the sensor output is amplified using an instrumentation amplifier for each axis. The INA128 instrumentation amplifier by Texas Instruments is used for this. The gain of the amplifier is set by an external resistor according to the relation

$$A = 1 + \frac{50k\Omega}{R_g} \tag{5}$$

Setting R_g to 100Ω equates to a gain of 501 which gives a dynamic range of about ±1.50V for a maximum field of 0.6gauss. In order for a microcontrollers ADC to process this value it needs to be offset such that all values are positive. For a 5V supply line an offset of 2.5V is applied to the output of the instrumentation amplifier. The INA128 has an offset reference pin and thus connecting a buffered a voltage divider sourced from the 5V supply line is sufficient to offset the output. The bandwidth of the INA28 at gain of 500 is less than 100KHz . An RC filter was used to limit this bandwidth to 1KHz to try and limit any noise in the circuit however problems with the ADC were encountered. The RC filter was removed and the output of the INA128 fed straight to the ADC.

A problem arises in using a large amount of amplification on the sensor output. The Wheatstone bridge of the sensor will have an offset value of up to ±11.25mV but typically somewhere around ±2mV. Furthermore, during sensor evaluation it was found that the offset is not always constant. Small fluctuations in this offset mean that a constant zero offset cannot be programmed into the microcontroller that samples these values in order to get a compass heading. It is therefore necessary for the microcontroller to perform a calibration of the sensor during initialization in order to properly determine the offset value.

When the sensor is exposed to large magnetic fields the resistive elements start to become magnetized which reduces the performance of the sensor over time. A reset strap is included to

negate the effects of any magnetizing fields. By applying a large negative current followed by a large positive current the sensor function is restored. The datasheet for the sensor suggests using a CMOS totem pole configuration to convert a pulse signal to the necessary currents required for a reset. The circuit is able to generate a -500mA current pulse for a minimum of 2μsec followed shortly after by a +500mA pulse again for a minimum of 2μsec. The reset straps for each axis (x and y) has an equivalent resistance of about 8Ω. The reset signal is a 5V digital pulse generated by the MCU microcontroller. The schematic is shown in Figure 11.
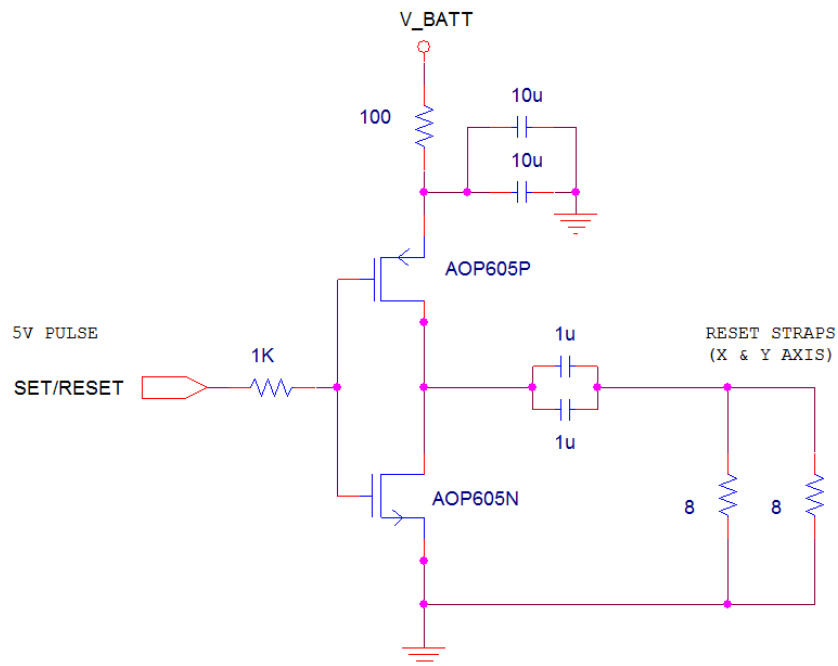
Figure 11: Schematic of CMOS totem pole circuit to drive sufficient current through magnetometers reset straps. Circuit will sustain a current greater than 500mA for at least 2μsec.

The AOP605 is a complimentary MOSFET IC package able to deliver pulsed currents of up to 30A and low gate voltage threshold of 1.8V. Using a 5V driver to pulse a current less than 1A is easy and convenient using this small IC. Suggested values for the tank and blocking capacitors are given in the HMC1022's datasheet however values were chosen through a combination of simulation and trial and error. The complete schematic for the analog interfacing of the magnetometer is shown in Figure 12.
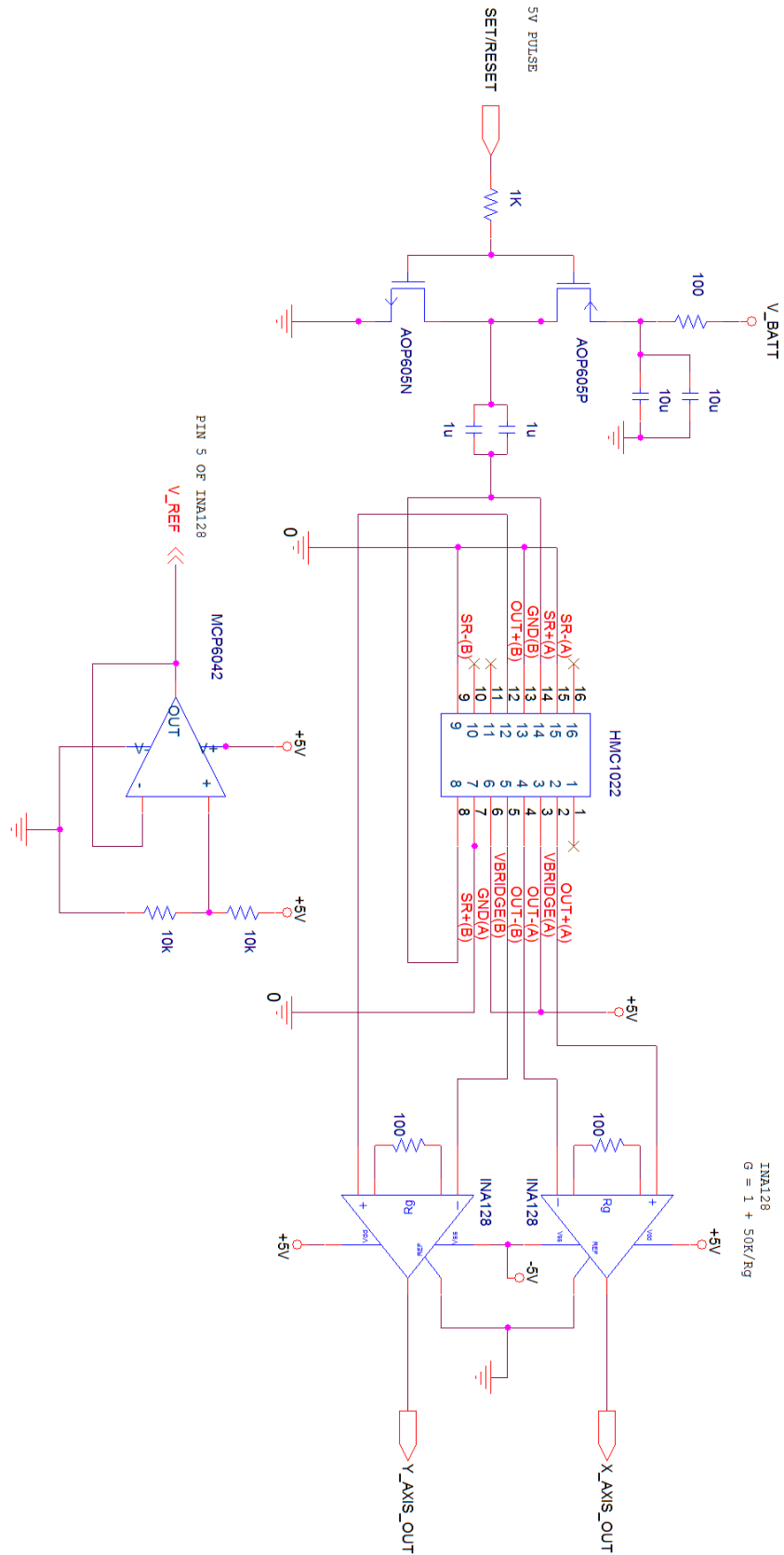
Figure 12: Complete circuit for interfacing with the HMC1022 magnetometer. The Set/Reset signal is a 5V pulse from the MCU microcontroller and the outputs of the circuit are to be sampled by the MCUs ADC. V_REF is used to add an offset to the INA128s output

4.4 TRAJECTORY MEASUREMENT UNIT: PEDOMETER

The pedometer is used to determine if a person is walking or stationary in order to avoid delivering unnecessary vestibular stimulation. Application Note 602 by Analog Devices [22] explains the design of a pedometer for measuring walking distance and speed using a single axis accelerometer. Since the TMU is not concerned with speed the design is greatly simplified.

A simple analysis of a persons' gait shows that when one foot is planted on the ground and the other lifted and moved forward, the hip of the moving foot is elevated by a small amount from the standing position. An illustration of this motion is shown in Figure 13.
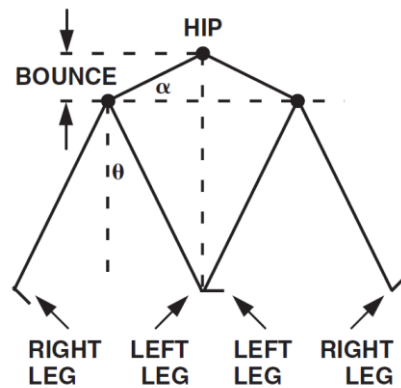
Figure 13: Vertical motion of the hip while walking. Image sourced from
Application Note 602 by Analog Devices [22].

This vertical movement can be quantified by an accelerometer in the vertical direction (z-axis). When this acceleration exceeds a set threshold a step is registered. The MMA1270EG is a single axis accelerometer capable of detecting forces up to $\pm2g$. The sensor comes as in IC package that filters, offsets and amplifies the signal such that it can be easily connected to a microcontroller with minimal additional circuitry. The zero gravity (zero-g) output of the sensor is 2.5V with a sensitivity of 750mV/g. When mounted in the vertical direction a constant force of 1g due to earths' gravity is experienced by the sensor. The threshold voltage required to register a step then should be greater than 3.25V.

A comparator module on the MCU microcontroller can be used to determine if the sensor output exceeds a set voltage. The threshold voltage is set using a voltage divider consisting of a fixed resistor value and a potentiometer. This allows for easy tuning of the threshold voltage. Additionally, AN602 suggests that the microcontroller processing the signal should insert a

dead-time after detecting a step. When the foot is planted back down onto the ground some bouncing in the signal may be observed. The dead-time helps prevent this bounce from registering a false positive. A complete circuit for the pedometer is shown in Figure 14. No buffer is required for the voltage divider network as the effective resistance of the microcontroller input is significantly higher than the 5kΩ potentiometer.
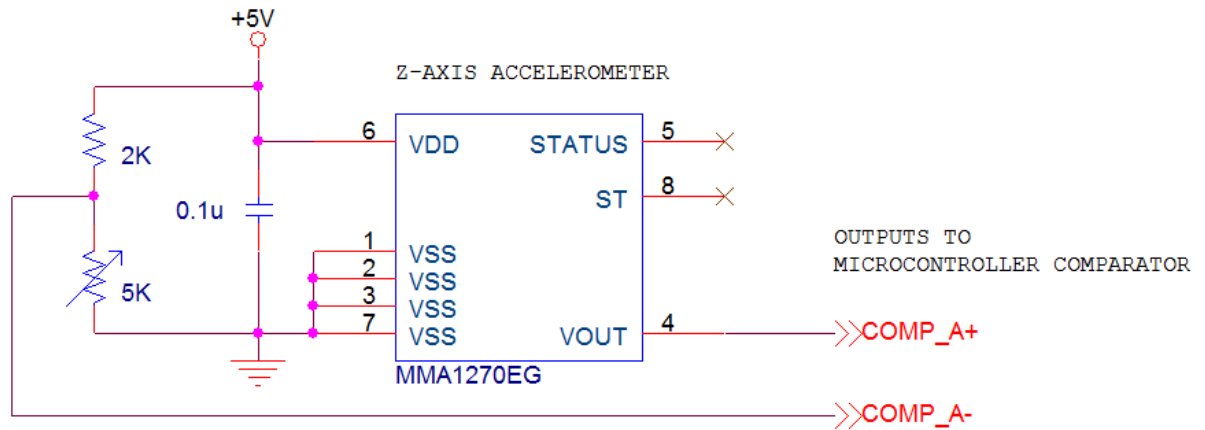
Figure 14: Complete schematic for interfacing of the MMA1270EG
single axis accelerometer to a microcontroller on-chip comparator.

4.5 MASTER CONTROL UNIT

The master control unit (MCU) needs to have an onboard CAN controller, ADC, comparator and DAC. The PIC18F4580 is an 8 bit microcontroller by Microchip Technology Inc that has these features with 32Kbytes of programs memory, 1.5Kbytes of data memory and processing speeds up to 10MIPS. Interfacing of the TMU to the controllers onboard ADC and comparator is outlined in sections 4.3 and 4.4 .The DAC is required to generate the analog waveform to control the current source delivering the vestibular stimulation. The PIC18F4580 has an onboard voltage reference module which uses a resistor ladder to generate an analog signal with a discrete magnitude. The resulting waveform is outputted to the voltage controller current source. Generating the waveform is outlined in section 5.4 .

The microcontroller also has what's referred to as an Enhanced CAN controller (ECAN). This protocol controller is programmed to generate and process the signals sent over a standard

CAN bus. The MCP2551 CAN Transceiver by Microchip Technology Inc acts as interface between the ECAN protocol controller and then physical CAN bus. Its purpose is to convert the digital signals generated by the ECAN controller into a differential signal suitable for transmission across the bus. According to the specifications for a physical CAN bus implementation [18], the ends of the bus must have a 120Ω resistance to reduce any signal reflections. Additionally the MCP2551 has an optional resistor that can be used to control the slew rate of the differential signal generated. Using the charts from the datasheet a value of 100kΩ is chosen to provide a slew rate of 5V/µsec. This reduction in slew rate reduces the amount of ringing noise across the CAN bus. The complete schematic of the MCU showing all interfacing connections to other subsystems is shown in Figure 16.

4.6 VIRTUAL SENSOR

In order to validate the system there must be some sort of sensor in the system reporting objects in its FOV. Since developing an array of sensors to detect physical objects is out of the scope of this project a series of virtual sensors are used to emulate an actual sensor. The sensor needs only to report the distance to an object at periodic update periods through the CAN bus.

The PIC18F2480 has the same functionality as the PIC18F4580 used for the MCU. It is an 8-bit microcontroller by Microchip Technology Inc that features 16Kbytes of program memory and 768 bytes of data memory. This is sufficient to run any code to simulate any amount of sensors. The microcontroller interfaces onto the CAN bus in the same fashion as the MCU by using the MCP2551 with the same slope control resistor and bus termination resistor.
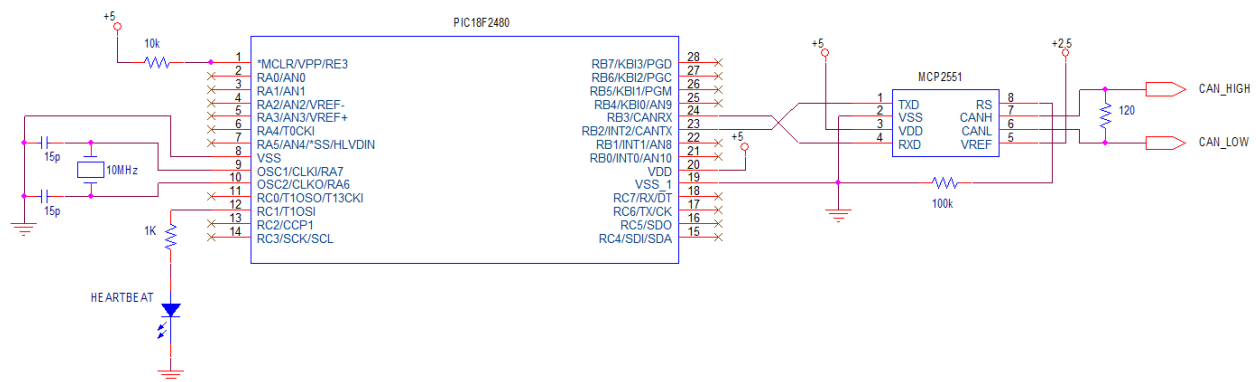
Figure 15: Schematic for Virtual Sensor
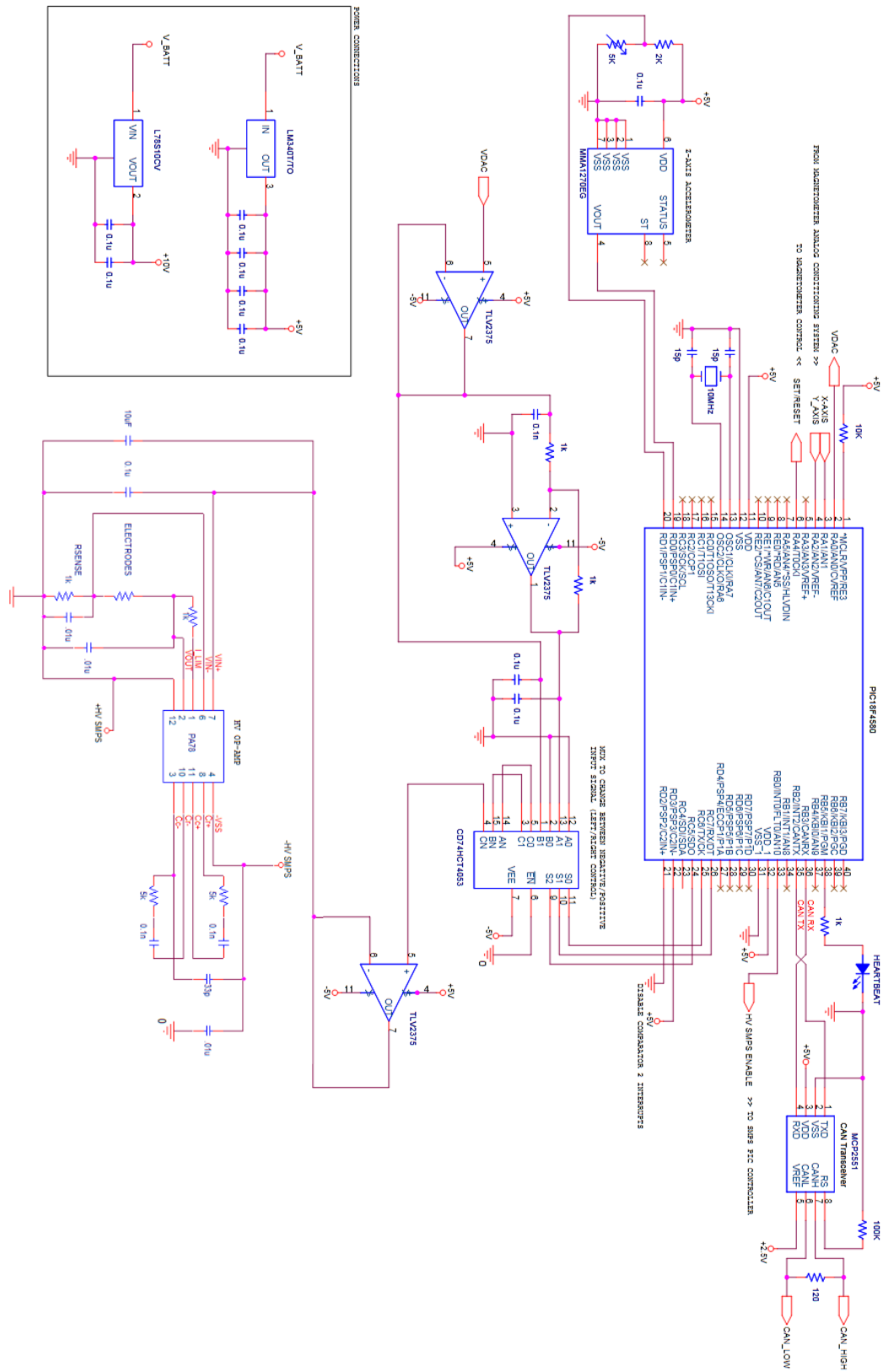
Figure 16: Complete MCU schematic indicating all connections to other subsystem circuitry and CAN bus

SYSTEM DESIGN: SOFTWARE

Algorithms along with software development notes are presented in this section of the report. Actual software source code is included as an appendix. All software was implemented on a PIC18F microcontroller platform using the C18 Tool suite provided by Microchip Technology Inc. Final development was done in the MPLAB IDE and programmed and debugged using the Microchip In-Circuit Debugger (ICD2).

5.1 COLLISION AVOIDANCE ALGORITHM

The collision avoidance algorithm designed here is a significantly simplified algorithm based on some of the key ideas presented in literary research done on the Nearness Diagram Method in section 2.2 . Objects detected by the sensors in the network are mapped into an array representing the 180 degree area in front of the user. The center of this 180 degree map is the current heading of the user (Heading) as obtained from the TMU and the limits extend to (Heading $\pm$ 90º) % 360º, where % is the modulo operator. Objects in this map are considered threats if their distance to the user is within a specified range. The algorithm then walks through each degree range in the map and determines how many objects are threats and what level of a threat they are based on their distance. Close objects pose higher threats then further ones. The closest object then sets the current threat level which is translated into an appropriate stimulation level. Higher threats require more magnitude deviation in walking trajectory and as such higher currents are delivered. If a threat exists then the algorithm must determine if moving left or right is the best option to avoid a collision. An example map with multiple threats is shown in Figure 17.
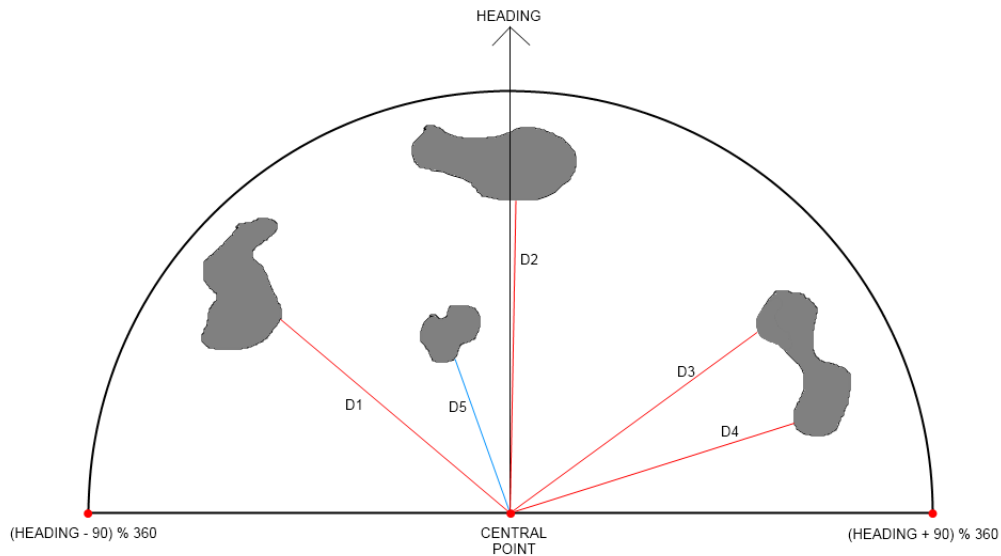
Figure 17: Conceptual Threat Map, 180 degree span. The closest object to the central point (D5) is the object that poses the most threat. Threat level is baed on this distance.

With threat level determined the algorithm then extracts all the headings with no impeding objects. A valley is defined as a sequence of consecutive headings void of any threats meeting a minimum defined size specified in degrees. Starting from the left, (Heading − 90) % 360, the algorithm will extract the first valley. It is referred to as the best current valley. The algorithm then proceeds to extract each consecutive valley until the end of the map is reached. Every valley extracted is compared to the current best valley and if it is deemed a better valley the current best valley is updated. The optimal valley is always the valley that has the current heading passing through it. If an optimal valley is not found then the best valley is the valley with the least distance from the current heading. Once the best valley is determined its direction is determined to be straight, left or right depending on its location with respect to the current heading. A conceptual map is of this is shown in Figure 18.
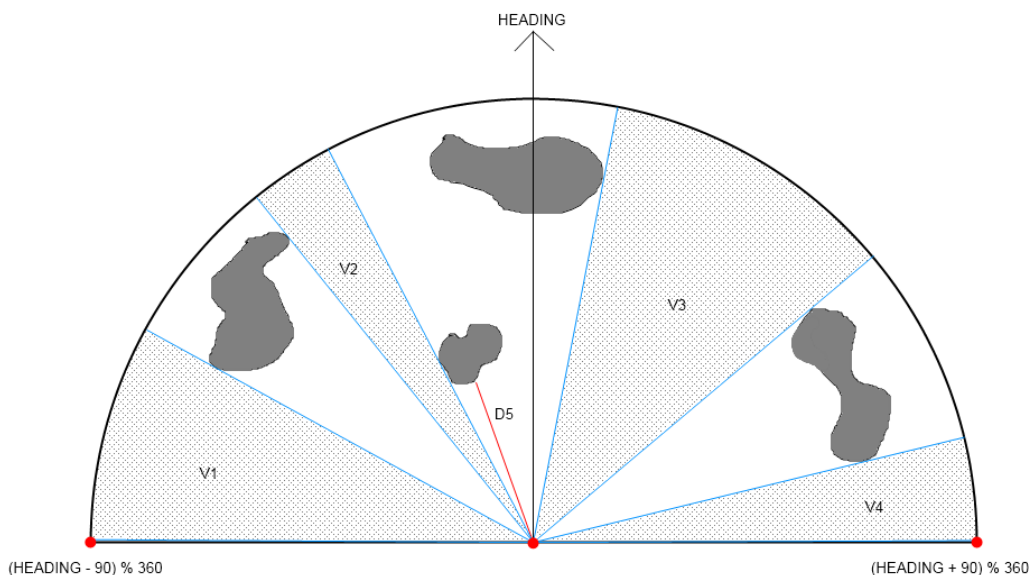
Figure 18: Conceptual Threat Map, D5 is the closest objet dictating the threat level. Extracted valleys in the map are V1 through V4. The best valley is V3 since it is closest to the current heading and so the direction of stimulation is to the right. V2 may not be a valid heading if it does not meet the minimum defined valley size.

Two additional angle spreads are now defined, the Forward angle and the Sweep angle. The forward angle is defined as the angle spread centered at the current heading in which objects are evaluated to determine the current threat level. Objects in the map outside the Forward angle are not taken into consideration when determining the threat level. The Sweep angle is defined as the angle spread which valleys are extracted from. This value should be greater than the Forward angle and less than 180 degrees. Figure 19 depicts the Forward and Sweep angle. The flowchart and some basic pseudo code for the algorithm are shown in Figure 20.
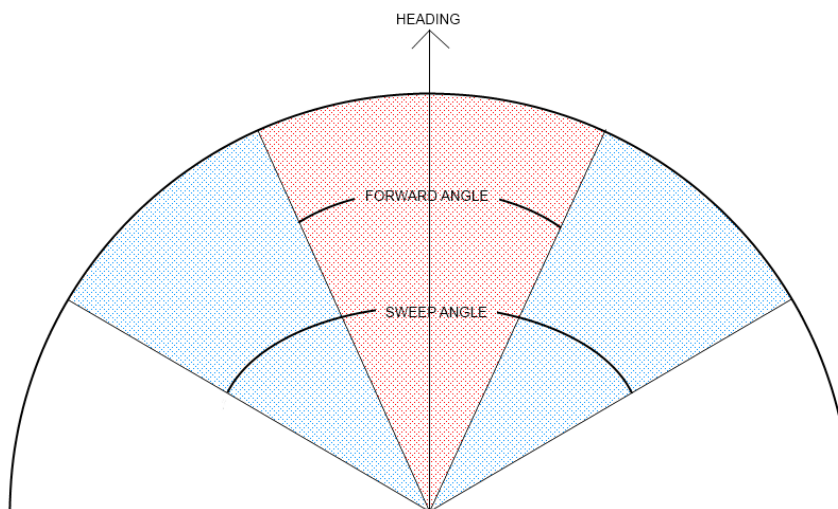
Figure 19: Conceptual Threat Map depicting the Forward Angle and the Sweep Angle

For (i = (HA – FA) : (HA + FA))
  if (TM[i] < Dist_Hi)
      Threat = High
  else if (TM[i] < Dist_Mid)
      Threat = Mid
  else if (TM[i] < Dist_Low)
      Threat = Low
  else
      Threat = None

For (i = (HA – SA) : (HA + SA))
  if (TM[i] > 0)
      valley_length++
  else
      evaluateValley
      valley_length = 0

ND Start

Threat Map (TM)

Heading Angle (HA)

Determine Threat Level

Forward Angle (FA)

Find Best Valley (Left, Right or Straight)

Sweep Angle (SA)

Return Threat Level
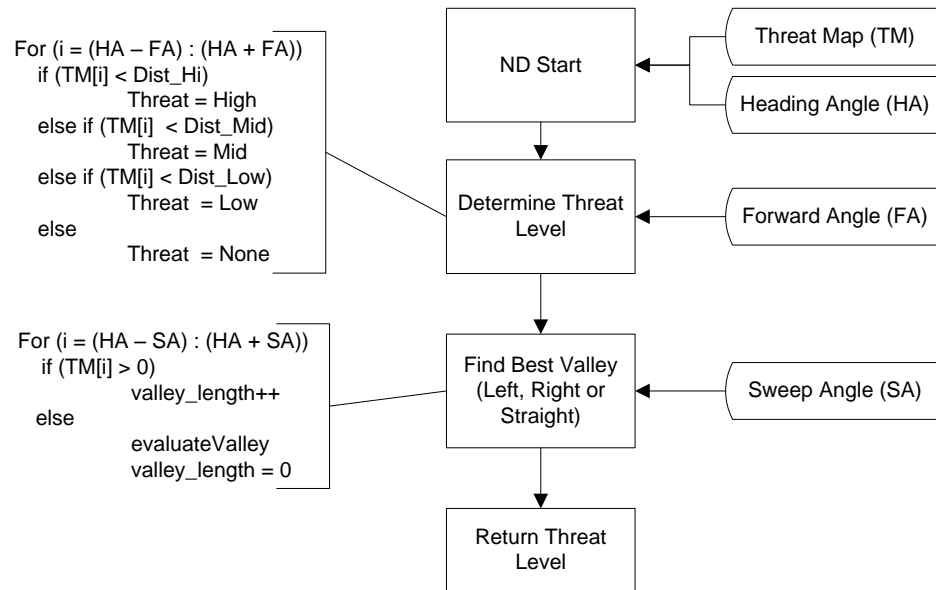
Figure 20: Flowchart for Collision Avoidance Algorithm

5.2 MCU Software: Overview

The MCU software is executed on the PIC18F4580 microcontroller. It is responsible for sampling the TMU, running the collision avoidance process, controlling the current stimulator and subsequent power supply and interfacing onto the CAN bus. The MCU runs on a 10MHz quartz crystal in High Speed PLL mode. This multiplies the clock frequency by a factor of 4 giving a total clock frequency of 40MHz. A flowchart of the MCU software is shown in Figure 21. The interrupt service routine (ISR) flow chart for the MCU is shown in Figure 22. The complete commented C code for the MCU is in Appendix D.

It should be noted that the navigation correction logic, used to correct a persons' trajectory to their default heading after all threats have been dropped, was not implemented due to complications in testing as well as time constraints.
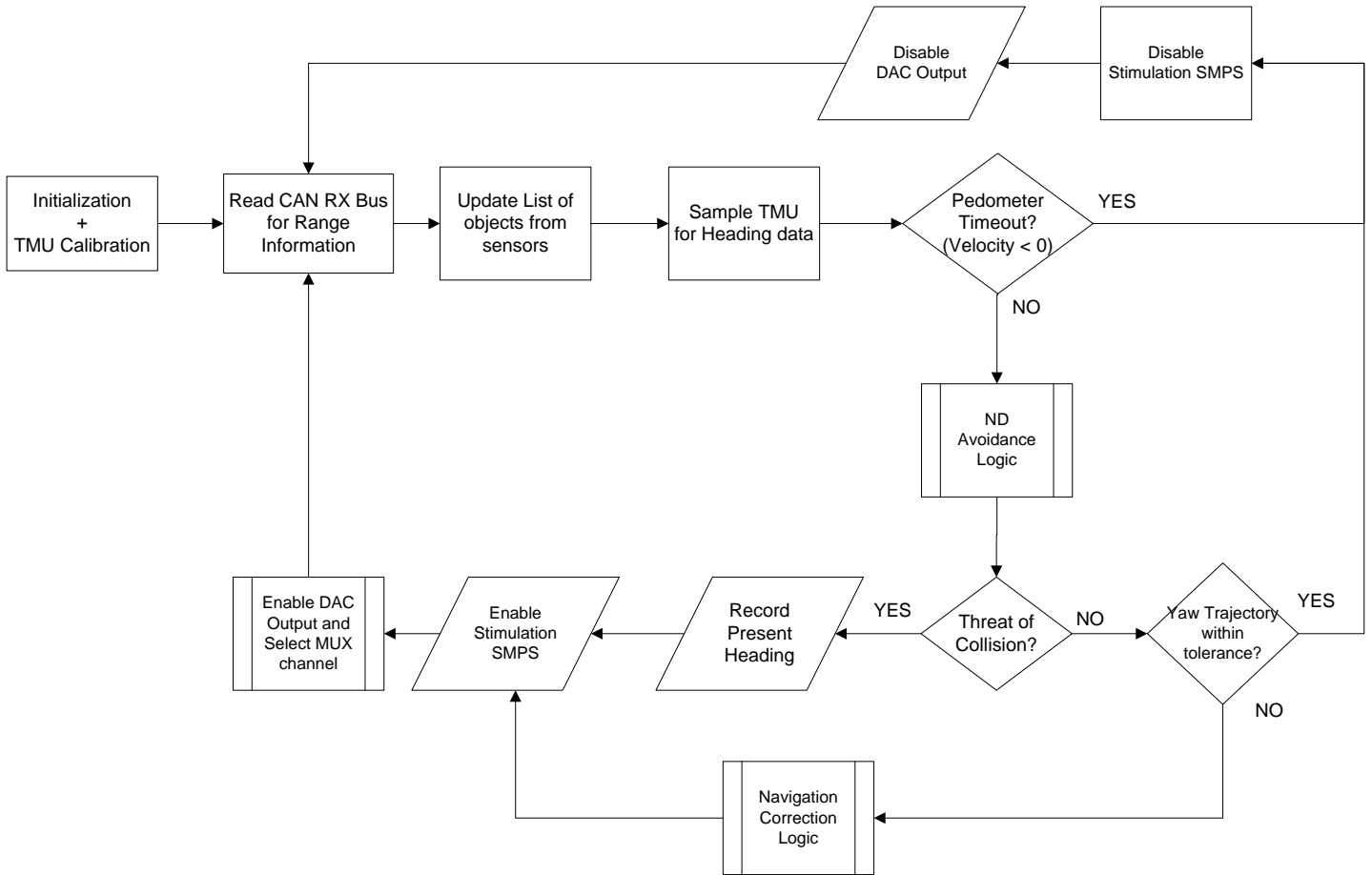
Figure 21: Software flowchart for Master Control Unit
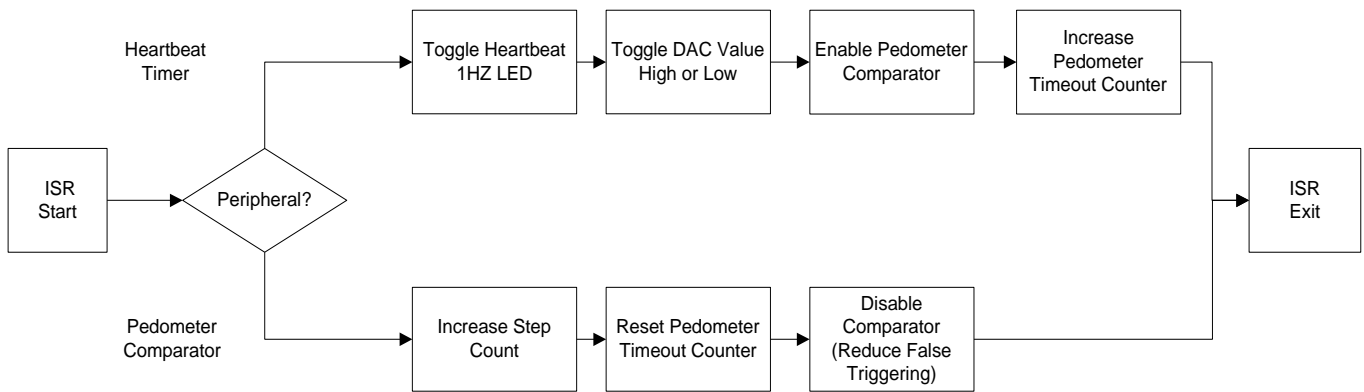
Figure 22: ISR Flowchart for Master Control Unit

5.3   MCU SOFTWARE: COLLISION AVOIDANCE IMPLEMENTATION

The data sent to the MCU by a sensor reports the sensors mounted position, Field Of View (FOV), sensor ID number and distance to an object. This data along with a time tag is stored as a structure and put into a list. The MCU maintains this list and removes any objects which have an expired time tag. New objects are added every time a new CAN message from a sensor is received.

When the Nearness Diagram (ND) Logic is called up the algorithm outlined in section 5.1 is executed. An additional step is required to run this algorithm. Object data is not stored as a large map array ready for processing but instead as a list of structures. An intermediate step is required to parse the structure list, extract relevant objects and build the map. Storing all time tag and distance data in an array requires more memory for a typical system then storing them in a list. The structures used to store sensor data contain 4 16 bit integers and a byte. Assuming a max list size of 20 objects the total memory required is 1.44kb. If data was stored directly as a threat map array of 180 elements (1 degree resolution map) then for a single element in the map one 16 bit integer is required for distance and another for a time tag. The total required memory is 4.32kb. Storing objects as a list then makes more sense in terms of memory consumption.

Distance reported by a sensor is a floating point value in meters however sending this data in a CAN message and storing it becomes a problem. Q scaling, see Appendix B for details, is used to store the floating point value as a 16 bit unsigned integer to save space and allow for transmission over the CAN bus. More about message transmission is presented in Appendix B.

Additionally the rate at which the ND algorithm is called up needs to be controlled in order to reduce hysteresis in the desired stimulation direction. If the algorithm is executed every iteration of the main program loop, then small perturbations in the magnetic sensors reading could affect the outcome of the algorithm. Since the time between two successive function calls is only a few milliseconds this can result in very rapid switching between positive and negative stimulation. To reduce the effects of this, a minimum time must elapse between ND algorithm calls. A value between 1-2 seconds was chosen but can easily be adjusted.

5.4   MCU SOFTWARE: GENERATING THE GVS CONTROL SIGNAL

The on-chip voltage comparator reference module (essentially a DAC) is used to create a square pulse waveform to drive the stimulation system. A 16-bit timer generates an interrupt, referred to as a heartbeat, every 0.42 sec (1:64 prescaler on 40MHz clock at 2^{16} counts). Every second heartbeat the DAC toggles its voltage between ground and a value proportional to the current threat level. This produces a signal with frequency 0.59Hz.

The criteria for enabling the SMPS and delivering a stimulating current are 1) threat level is high, medium or low 2) the pedometer has not timed out 3) stimulation direction is left or right. If all of these criteria are met then the DAC is turned on and the SMPS enable line set high. If one of these criteria is not met then the DAC is turned off and the SMPS enable line set low. In either event the value loaded into the DAC register that controls the amplitude of the pulse wave is constantly updated with every second heartbeat.

5.5   MCU SOFTWARE: CAN CONTROLLER

The PIC18F4580 has an on-chip Enhanced CAN (ECAN) controller. The controller allows for the device to operate in different modes providing enhanced message filtering capabilities, additional programmable message buffers and slight variations in message queuing. The MCU will run the ECAN controller in Mode 2 which uses 8 receive buffers to implement a FIFO for received messages.

The baud rate for the controller is considered next. The standard baud rate for a CAN network is 125kbit/s but can run as high as 1Mbit/s for newer controllers. Higher baud rates require precision oscillators and shorter distances between nodes. For this system 125Kbit/s is sufficient for the amount of data being transferred. The maximum number of bits in a message is 108 [18]. If a node is sending a new message frame at a frequency of 30Hz then the bit rate is 3240 bit/s. At a maximum bit rate of 125kbit/s a maximum of 38 nodes can be implemented in the system. A typical system should have less than 10 sensors so a 125kbit/s is a sufficient baud rate. The bit rate is generated using the following formula obtained from the PIC18F4580 data sheet [25]:

$$Nominal\ Bit\ Period = T_q * (Sync_{seg} + Prop_{seg} + Phase1_{seg} + Phase2_{seg}) \tag{6}$$

Where the time quanta T_q is defined in terms of the Baud Rate Prescaler (BRP):

$$T_q = \frac{2*(BRP+1)}{F_{osc}} \tag{7}$$

The bit is sampled by the controller between Phase1$_{seg}$ and Phase2$_{seg}$. Sampling the bit somewhere in the middle of the period after any transients have settled and well before the next bit to avoid errors due to consecutive high or low bits is ideal. Sync$_{seg}$ is always 1T$_q$ by definition and Prop$_{seg}$ is chosen as 1T$_q$ since the distance between nodes is very short relative to the distances CAN is designed for. Phase1$_{seg}$ and Phase2$_{seg}$ are chosen to both be 7T$_q$ so that the bit is sampled 1T$_q$ past the center of the bit period. The total number of segments per bit is then 16. For a bit rate of 125kbit/s a T$_q$ of 0.5µsec is required. The effective oscillation frequency of the MCU is 40MHz and so the BRP is selected to be 9.

Implementing the rest of the CAN control is done using the C drivers provided by Microchip Technology in Application Note 878 [23]. No message filters or masks are used since the MCU has to process all messages sent to it. Definitions on how to communicate data to the MCU is outlined rigorously in Appendix B.

5.6 VIRTUAL SENSOR

The virtual sensor uses the same CAN drivers as the MCU as well as the same baud rate settings. The algorithm for the software executed in this node is shown in Figure 23. Two sensor types were developed one referred to as a static sensor and the other dynamic. The static sensor simply monitored the navigation data broadcasted by the MCU. When a certain number of steps were taken, each virtual sensor broadcasts to the MCU predetermined distance values intended to stimulate a person left or right. Once a certain amount of steps are exceeded the broadcasting stops. This was the simplest type of sensor that could be used to confirm basic system functionality.

Basic Program Flow

Dynamic Sensor
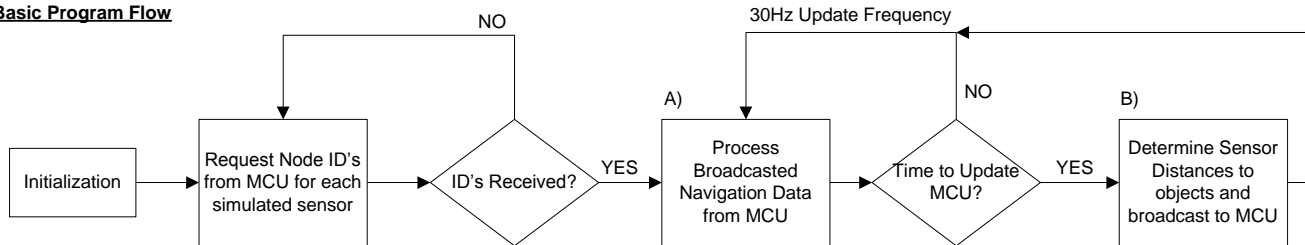
A) NAV Data Processing
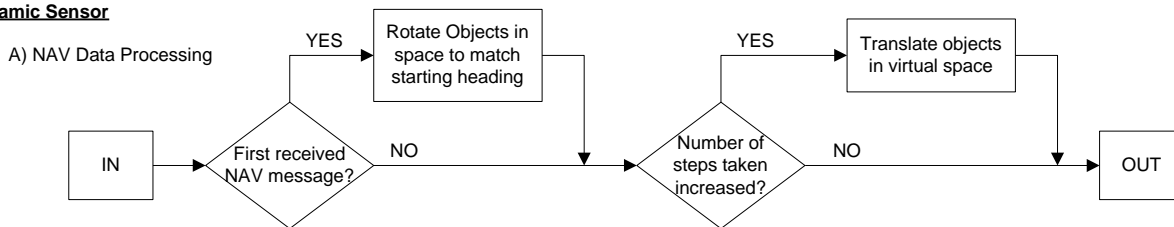
B) Determine Sensors Distance to Objects
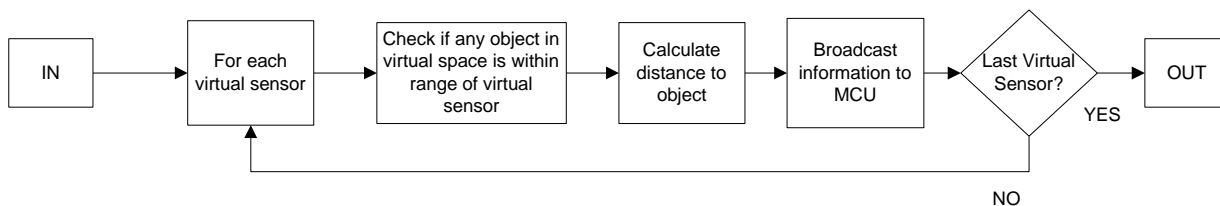
Static Sensor

A) NAV Data Processing
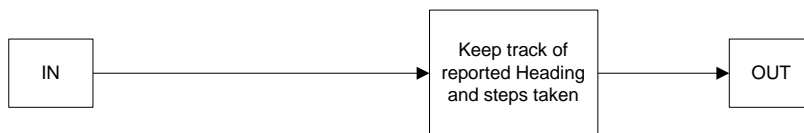
B) Determine Sensors Distance to Objects
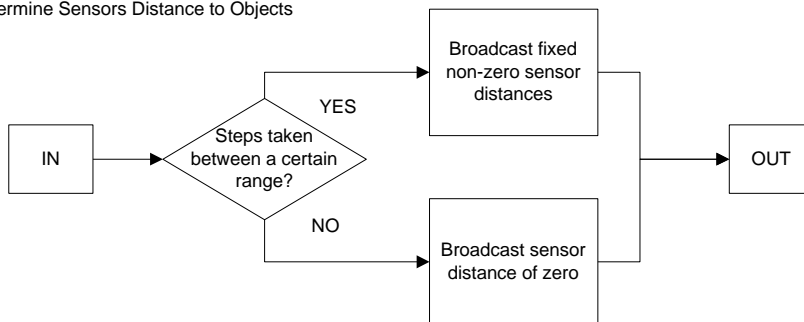
Figure 23: Software Flow and Algorithm for Virtual Sensor

The dynamic sensor is considerably more complex than the static one. Objects are placed throughout a virtual environment at fixed positions. As the person moves the object locations are translated in space to simulate movement through this environment. When it comes time to broadcast an update to the MCU each virtual sensor checks if any objects are within its FOV. If so the distance to the nearest object is calculated otherwise a zero distance is sent to indicate no objects were detected.

The objects are laid in a Cartesian plane with an assumed fixed initial heading. For example, if the assumed heading is 90° then an object located at [0,2] would indicate an object 2m directly ahead. When the virtual sensor receives a navigation message indicating the first step has been taken by the user, all objects are rotated in space such that they are oriented to the users initial trajectory heading. This is done by multiplying each object position [x,y] by a rotation matrix as a function of the angular distance 'θ', between the assumed heading and the heading reported by the MCU.

$$[X_{new}\ Y_{new}]^T = \begin{bmatrix} cos\theta & -sin\theta \\ sin\theta & cos\theta \end{bmatrix} * [X_o\ Y_o]^T \tag{8}$$

For every subsequent step taken the object locations are translated in space to reflect the movement by the user. Each object is translated by a constant distance 'r', indicative of a persons' step size in the opposite direction of the reported heading angle '¥'.

$$X_{new} = X_o + r * cos\left(\frac{(¥+180°)*\pi}{180°}\right) \tag{9}$$

$$Y_{new} = Y_o + r * sin\left(\frac{(¥+180°)*\pi}{180°}\right) \tag{10}$$

To determine if an object is within the sensors FOV the angle Φ which indicates the center angle of the sensor with respect to magnetic north, is found first. The value $Sensor_{start}$ is a positive or negative angle which defines an edge of the sensors FOV with respect to the mounted position on the user. A more detailed description of this angle and angle $Sensor_{width}$ is given in Appendix B.

$$\Phi = \alpha - \left(Sensor_{start} + \frac{Sensor_{width}}{2}\right) \tag{11}$$

If Φ is greater than 360 then subtract 360 from it. If less than zero then add 360 to it. The angle α indicates an objects (defined by position [x,y]) angle with respect to magnetic north.

$$\alpha = 90 - \text{atan}\left(\frac{x}{y}\right) * \frac{180}{\pi} \ for \ y > 0$$

$$\alpha = 270 - \text{atan}\left(\frac{x}{y}\right) * \frac{180}{pi} \ for \ y < 0$$

$$\alpha = 0 \ for \ y = 0, x > 0$$

$$\alpha = 180 \ otherwise$$

(12)

To determine if an object is within a sensors FOV then simply find the absolute difference between α and Φ and take minimum of result or 360 minus the result. If the calculated value is within the sensor width then it is within the FOV of the sensor. The distance to the object is easily found using basic trigonometry. The calculated floating point value is then scaled and broadcasted to the MCU.

$$Distance = \sqrt{x^2 + y^2}$$

(13)

HARDWARE TESTING AND SIMULATION RESULTS

Simulations of circuits were done using OrCad Capture. Models used in the simulations are PSspice models obtained from the manufacturers' website and imported into the environment. Circuit measurements were taken using a Tektronix digital oscilloscope. The results for different sub circuits are presented in this section.

6.1 SMPS

The circuit used for simulation in Capture is shown in Figure 24. A high impedance load of 50kΩ is used for simulation. No feedback is implemented in the circuit and the driver FET signals are set to match the timing from the microcontroller. A model for the IRFU9310 PMOS transistor was not available. The FQD2P40 has similar specifications to the IRFU9310 and was used in the simulation instead. The model was obtained from Fairchild Semiconductor.
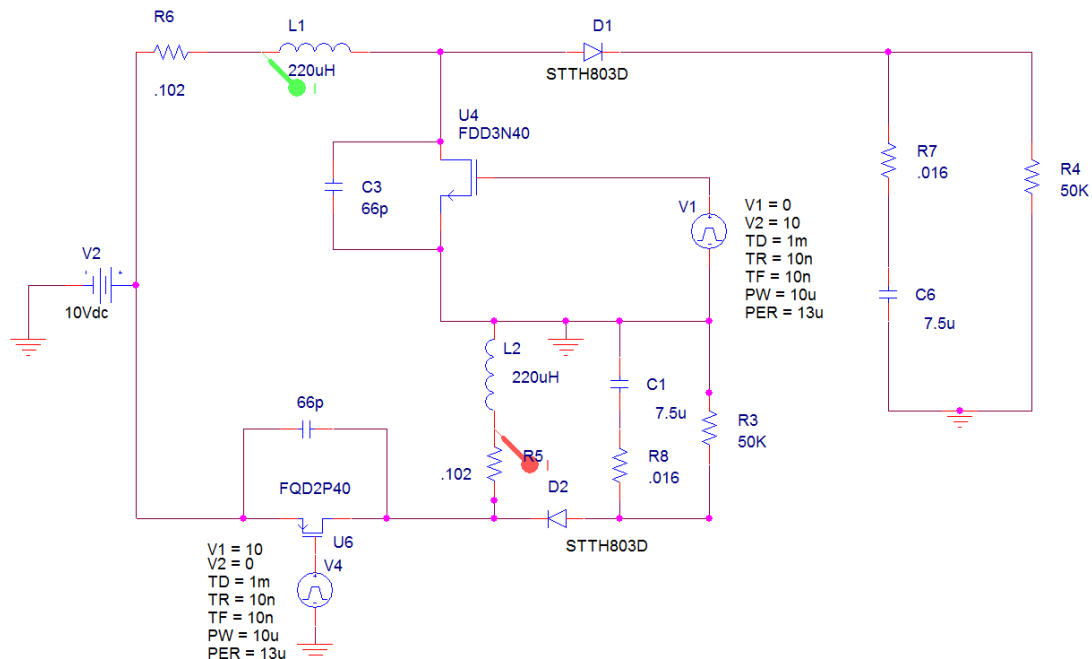
Figure 24: Simulation circuit SMPS

The simulated and measured output voltage over the load resistance is shown in Figure 25. In simulation, the target of 100V is reached in under 50msec however since no feedback control is implemented the voltage is unregulated and continues to increase with time.
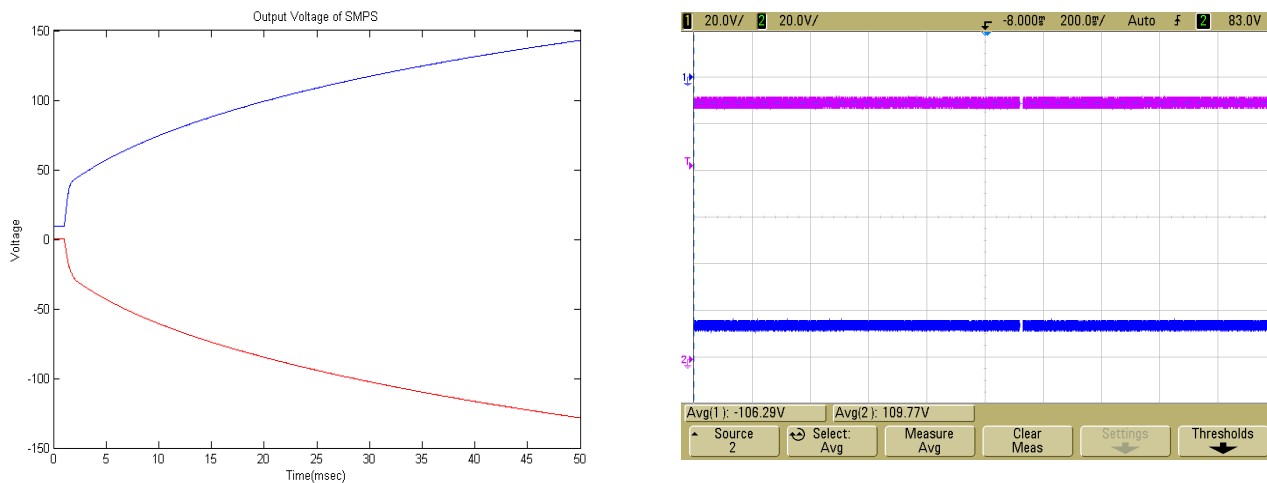
Figure 25: Left) Simulated output of SMPS. Right) Measured Output of SMPS

A large amount of noise is present on the output of the SMPS. This noise is mostly due to sharp transients and ringing due to the rapid switching of the transistors. The bypass capacitors used significantly reduce the amount of ringing as does the use of a perforated breadboard as

opposed to a solderless one. Noise could further be reduced using good layout techniques on a multilayer PCB however such a board is out of the scope and budget of this project. The noise present on the positive high voltage line and the effects of the bypass capacitors on the switching transistors shown are shown in Figure 26.
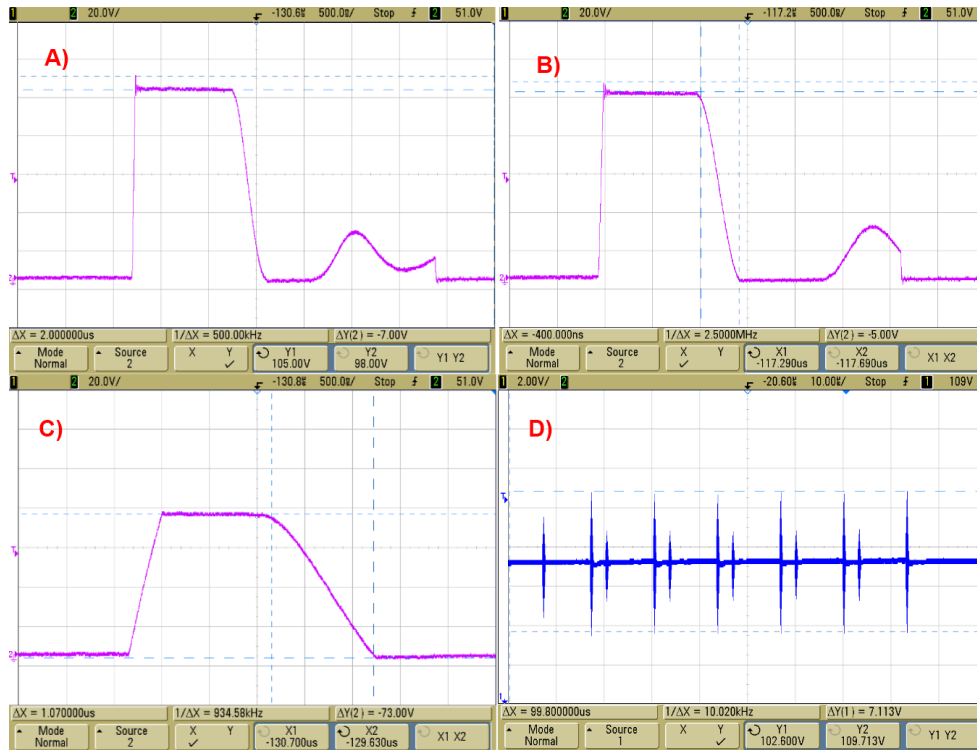
Figure 26: Voltage across switching transistor FDU3N40 with A) No bypass capacitor B) 66pF bypass C) 1nF bypass. D) Switching noise in output voltage of SMPS

Without use of a bypass capacitor overshoot in the transient is 7V. With a 66pF bypass this value reduces to less than 5V without affecting the fall and rise times of the transistor significantly. Higher bypass values such as 1nF almost completely reduce the amount of overshoot and ringing however the rise and falls times are affected such that the device no longer operates in discontinuous mode. With the 66pF bypass the current is able to completely discharge onto the capacitor in about 2.1µsec leaving the circuit is discontinuous mode for 1.9µsec as shown in Figure 27.
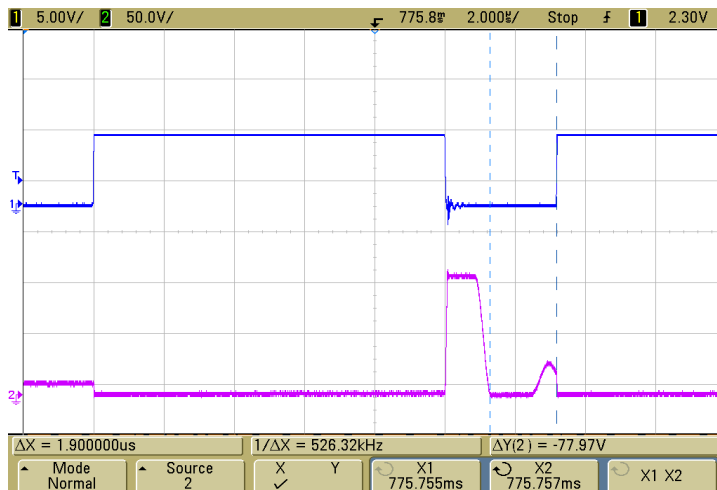
Figure 27: SMPS in discontinuous mode for 1.9μsec leaving 2.1μsec to discharge the current in the inductor. Blue) PWM signal from PIC18F1230, Red) FET voltage with 66pF bypass capacitor.

6.2 CURRENT CONTROLLED STIMULATOR

The circuit used for the simulation of the GVS current source is shown in Figure 28.
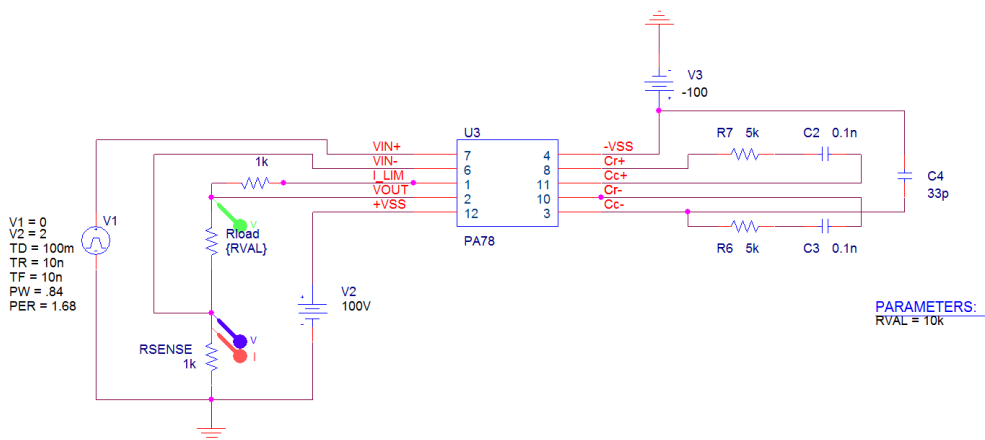
Figure 28: Simulation Circuit for GVS current source

A ±2V input signal is used with an expectant output of 2mA across the sense and load resistor. The simulated results are shown in Figure 30 and the measured results in Figure 29.
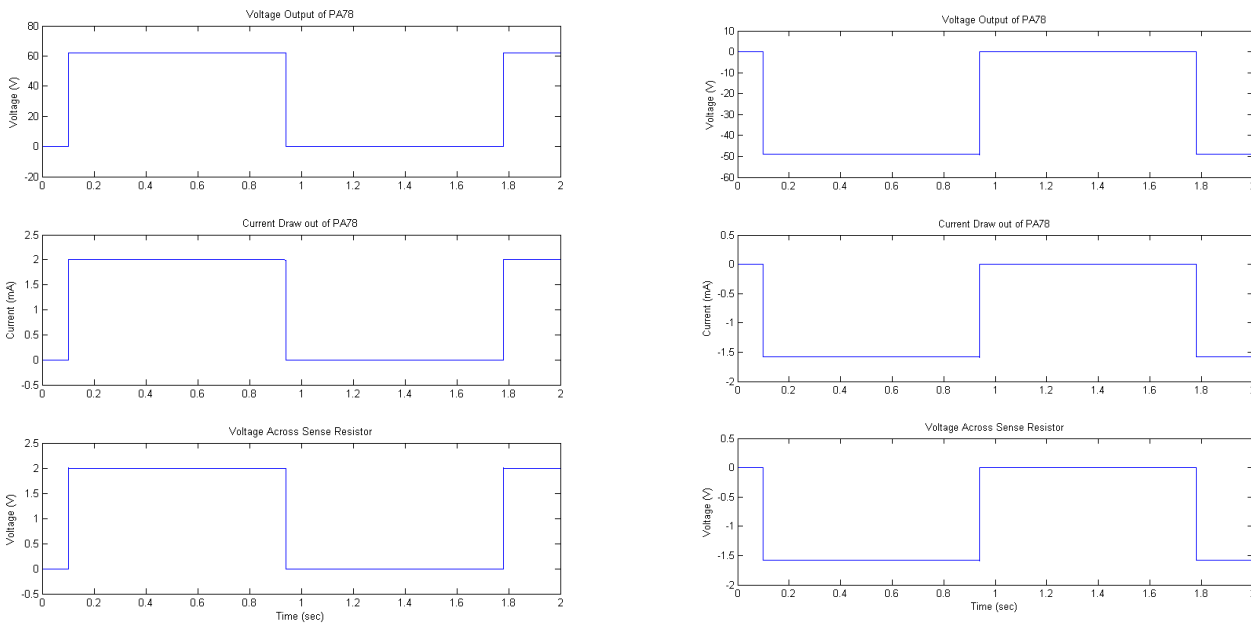
Figure 30: Voltage and Current output for simulated GVS current source with +2V input (Left) and -2V input (Right) over 10kΩ load
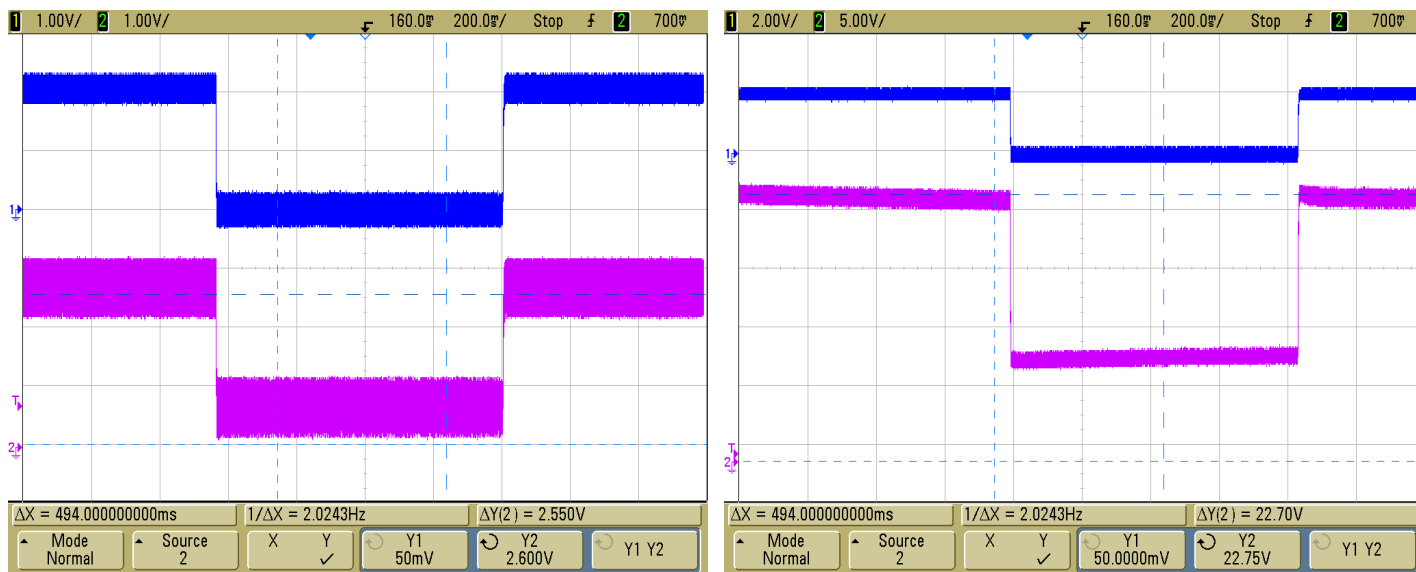
Figure 29: Voltage output for actual GVS current source using PA78 over 10kΩ load. Input is +2V signal from MCU DAC (Blue). Purple is V_{in}- (Left) and V_{out} (Right)

A large discrepancy between the simulated and measured results exists due to an offset in the feedback voltage. Regardless of the load impedance there is always a 725mV offset between $V_{in}+$ and $V_{in}-$ of the PA78. As the load increases so does the amplifier gain meaning this offset grows to very large values. The offset in V_{out} is almost 10V for the 10kΩ load. This offset also poses problems when trying to drive a negative current through the load. The resulting data shown in Figure 31 indicates that the input offset of the PA78 makes it almost completely useless for bipolar stimulation. Rather than try and correct for this bias, the resulting amplitude of the PA78 output was analyzed when the circuit was connected to a subjects' mastoid process to obtain a value of the approximate impedance of the tissue electrode interface.
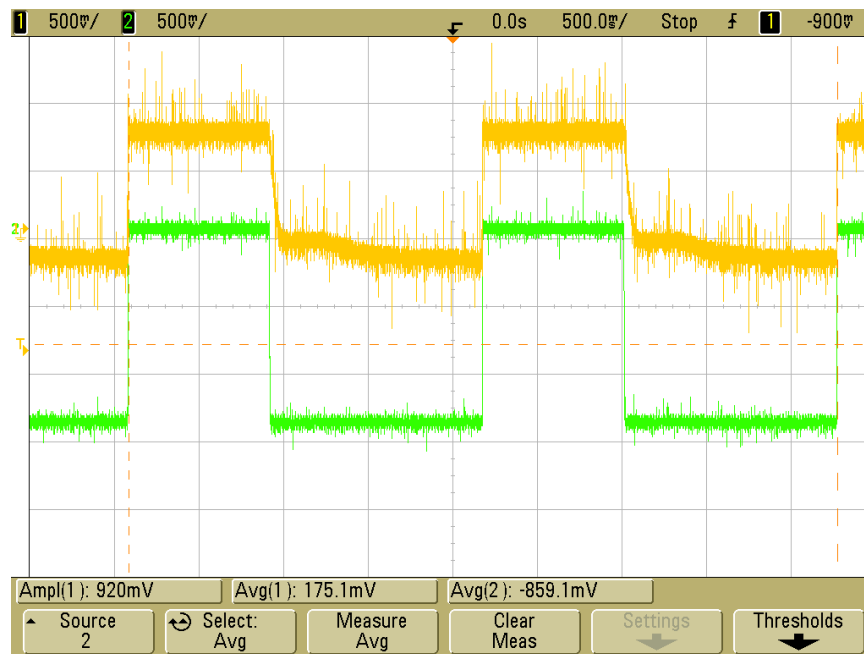
Figure 31: Negative Input to PA78 Current Source. -1.5V DAC Signal (Green) $V_{in}-$ of PA78 (Yellow).

Gold electrodes 1cm in diameter, were connected to a subjects mastoid process. The skin was cleaned using isopropyl alcohol and a generous amount of Ten-20 conductive gel applied between the electrodes and treated skin. A 2V signal was generated from the MCU and the voltage at V_{out} of the PA78 measured. For this setup the sense resistor in the circuit was changed to 2kΩ. The resulting waveform shown in Figure 32 indicates that the actual voltage required to drive a 1mA current through the tissue electrode interface is less than 6V indicating an impedance of less than 6kΩ.
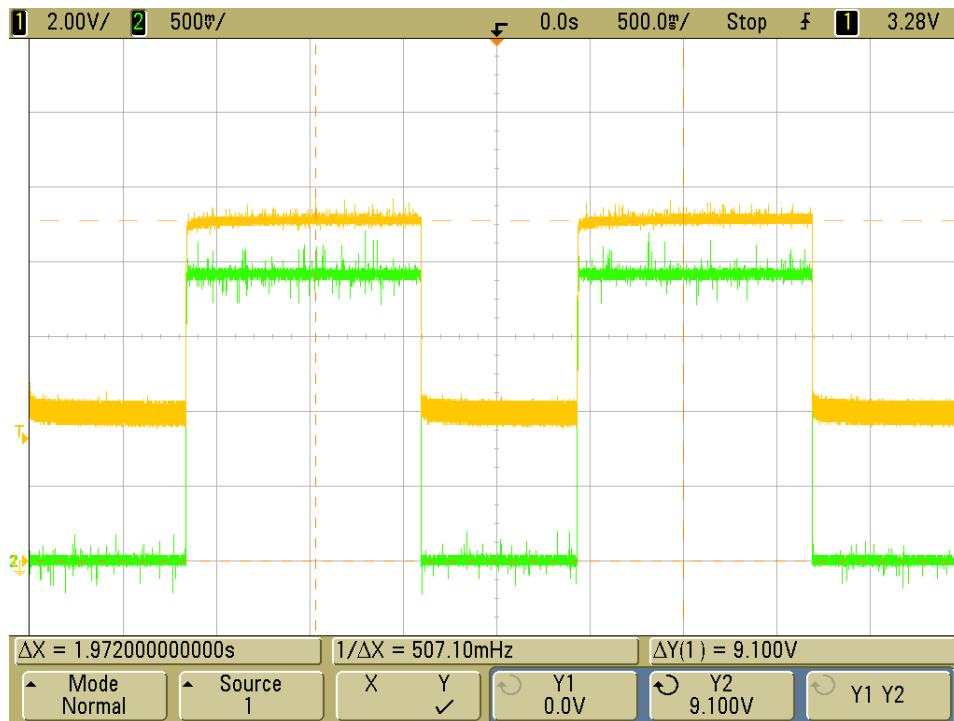
Figure 32: GVS Circuit connected to mastoid process. Input is 2V signal (Green).
Output at V_{out} of PA78 is shown in Yellow.

This measured impedance is significantly lower than what was expected during the design phase of this project. In light of this the PA78 was replaced with a different op-amp, the OPA445 from Texas Instruments. The OPA445 is a precision high voltage amplifier capable of handling supply rails up to ±45V. The PIC18F1230 used in the SMPS was reprogrammed to regulate the output to ±42.5V and the OPA445 connected in place of the PA78.
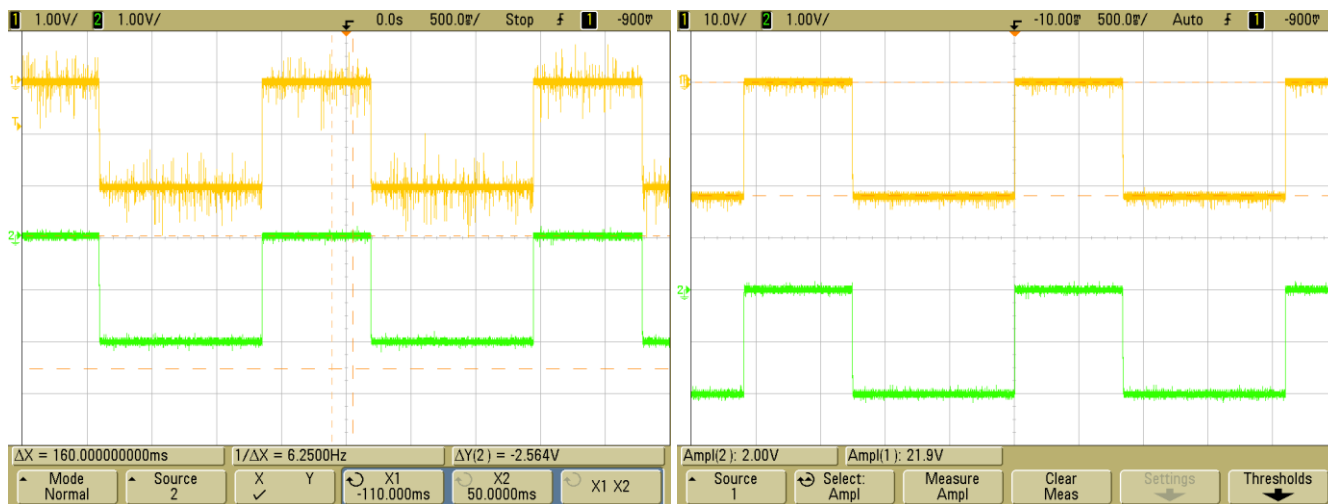
Figure 33: OPA445 voltage over 10K load with -2V signal.
Green is DAC signal, Yellow Left: V_f. Yellow Right: V_{out}

With the OPA445 the offset bias seen with PA78 is no longer an issue and the measured results shown in Figure 34 closely match the simulated results. The stimulation unit using the OPA445 was connected to a subjects mastoid processes and a 1mA current applied. The stimulation results shown in Figure 34 have no voltage offset and a reduced discomfort during stimulation compared to the PA78. The effects of the GVS are experienced as dizziness and disorientation when the subjects eyes are open however since the applied voltages are lower in magnitude the amount of discomfort experienced due to electrical stimulation is significantly reduced.
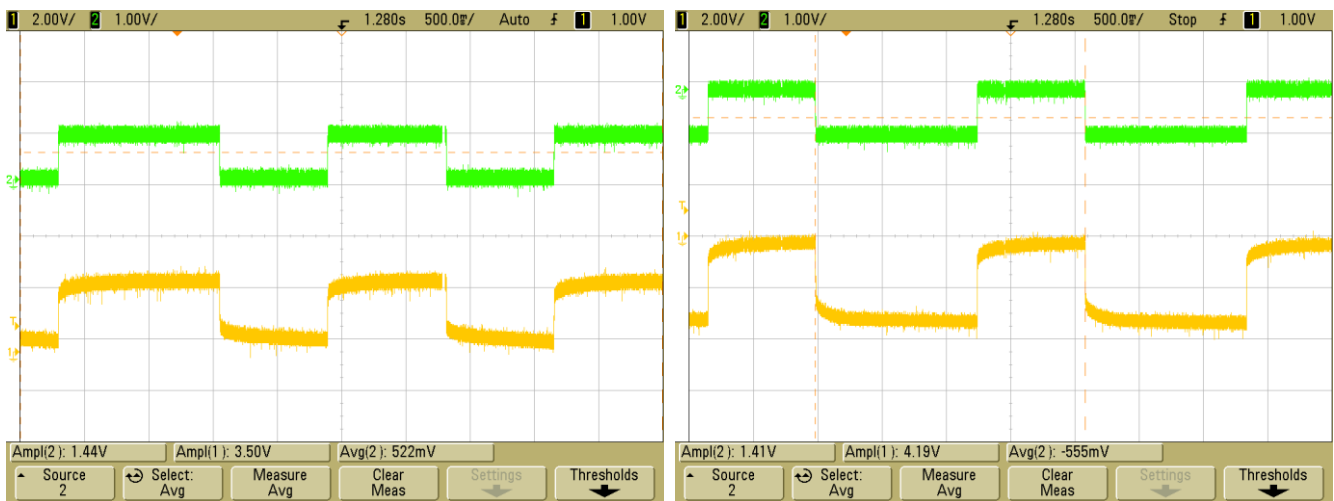
Figure 34: OPA445 Simulation over Mastoid Processes at 1mA of current. Green is V_f and Yellow V_{out} of op-amp. Left is for positive stimulation and Right negative stimulation

6.3   MAGNETOMETER & RESET PULSE CIRCUIT

The circuit used for simulation of the reset pulse circuit is shown in Figure 35. The pulse generated by the MCU is a 5V digital pulse 144μsec in duration. The simulated results, Figure 36 indicate a peak current delivery of almost 800mA on each reset strap. The current spikes are greater than 500mA in magnitude for approximately 4μsec which exceeds the 2μsec duration required in the datasheet for the HMC1022.

The measured waveform shown in Figure 37 indicates that the voltage over the reset straps is sufficiently high to deliver the 500mA current pulse for at least 2μsec. The effects of the pulse are observed in the x and y outputs of the magnetometer shown in Figure 37. When the negative pulse is applied the output switches polarity about the zero position. The positive pulse that

follows then restores the sensors output to its default polarity removing any magnetization affects accumulated due to exposure to large fields.
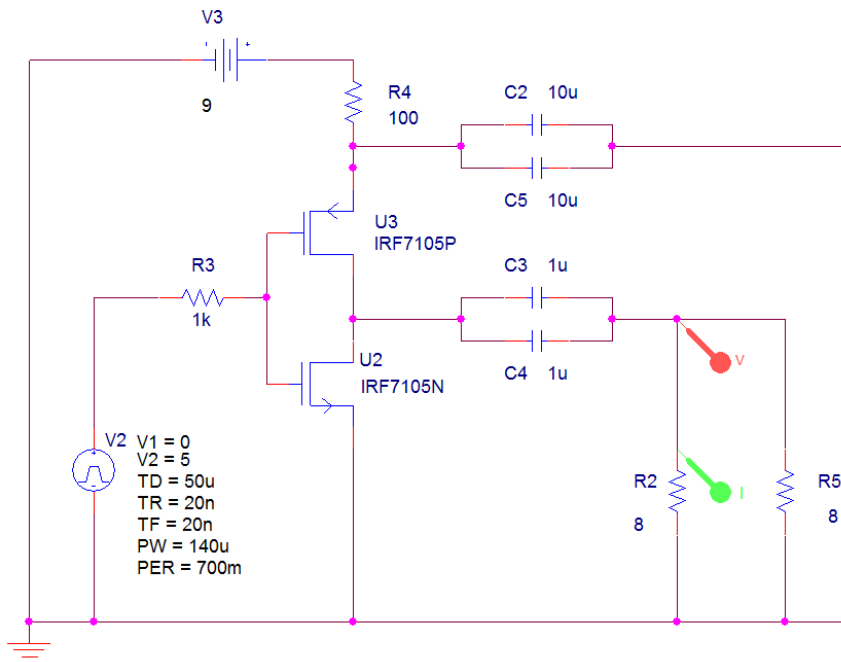
Figure 35: Simulation schematic for Magnetometer reset pulse
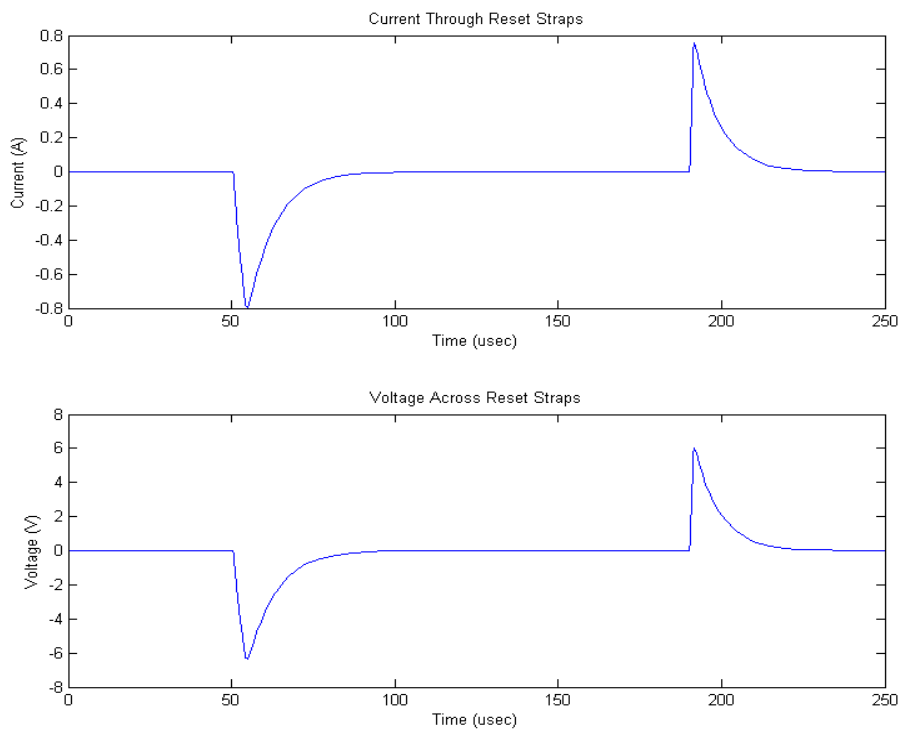
Figure 36: Simulation results for Magnetometer reset pulse circuit
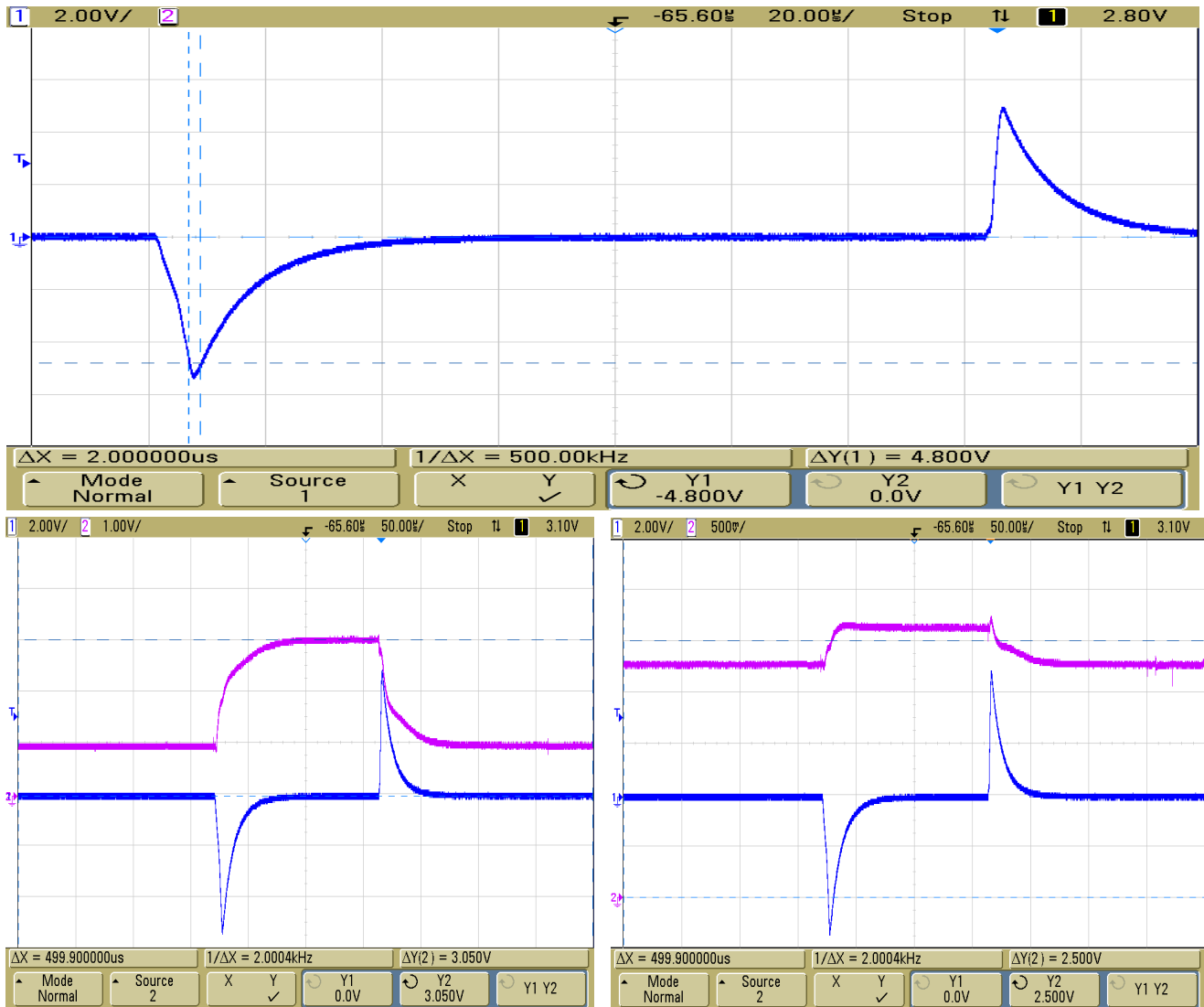
Figure 37: Measured results of Magnetometer reset pulse circuit. Top: Voltage drop over reset straps. Bottom: Purple indicates amplified sensor output for X axis (Left) and Y axis (Right)

The voltage range of the amplified output of the HMC1022 for both X and Y axis was theoretically supposed to be ±1.5V for a gain of 501 on the INA128 as discussed in section 4.3 . In actuality the output range was only ±0.35V. The discrepancy between the calculated and measured range is most likely due to the use of solderless breadboard and numerous jumped wires used to interface the INA128 to the HMC1022. The unamplified signal is less than 5mV and when passed through a noisy plane could be reduced enough to cause the observed discrepancies in signal intensity. To compensate for this the INA128 had its gain boosted to 1000

to give an output range of ±0.7V in order to reduce some of the quantization error of the ADC. During bench testing however the heading values as read from the PIC18F4580 using the in-circuit debugger tended to fluctuate about 3 degrees for a fixed sensor position.

6.4 PEDOMETER

The sensitivity of the MMA1270EG is 750mV/g at a 2.5V zero-g offset. The expected voltage level to detect a step should be at about 3.25V with the axis of the sensor mounted vertically along the hip of the user. The measured waveforms taken during a heavy over accentuated step and a regular step with the pedometer mounted at the left hip are shown in Figure 38.
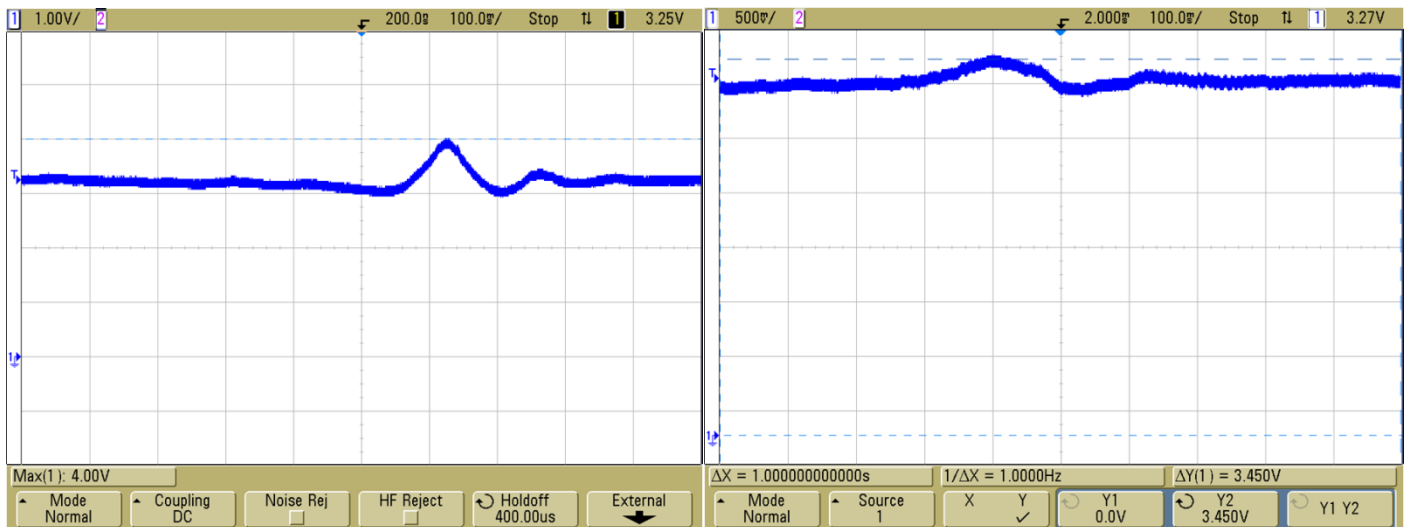
Figure 38: Measured response of MMA1270EG during a heavy step (Left) and a regular step (Right)

The baseline voltage was measured to be at around 3.2-3.3V due to small motions while the left foot was planted on the ground. For a heavy step the peak voltage is as high as 4V but for a regular step the voltage is at most 3.45V. This leaves a very small margin for accurate step detection.

The reference voltage generated using a voltage divider along with the signal from the MMA1270EG is fed into an on-chip comparator on the MCU. While an ideal reference voltage of 3.4V should be used according to the measurements it was found that in order to accurately

detect steps this voltage needs to be lowered. The 5kΩ potentiometer was adjusted through trial and error to a value that would accurately detect steps. The reference voltage was set to 3.31V.

SOFTWARE & SYSTEM VALIDATION

7.1 NEARNESS DIAGRAM ALGORITHM

The algorithm was initially designed in MATLAB to ease testing and debugging. The developed code was then rewritten in C using the MinGW tool chain and the Eclipse IDE, a free open-source Integrated Development Environment. Simulated test cases were done in Eclipse and the output of the algorithm verified against theoretical expected results. The source code used for testing is included in - Software. Test cases and results are outlined in Table 1. The values of the Forward and Sweep angles used were 10 and 30 degrees respectively. Security zones were 2m for high threats, 4m for mid level threats and 6m for low level threats. For a description of the values θ_{min} and θ_{width} see Appendix B.

Table 1: Test cases and results for validation of collision avoidance algorithm

Test Case	Num of Threats	Heading (deg)	θ_{min}	θ_{width}	Reported Distance	Output Direction	Output Threat Level
1	1	360		10	3.456m	Right	Mid
		360	-5	11	3.456m	Left	Mid
		360		12	3.456m	Left	Mid
2	1	350			3.456m	Left	Mid
		345			4.456m	Left	Low
		344	-5	11	4.456m		No Threat
		10			1.15m	Right	High
		15			3.456m	Right	Mid
		16			4.456		No Threat
3	1	180		10		Right	Mid
		180	-5	11	3.456m	Left	Mid
		180		12		Left	Mid
4	1	190				Right	Mid
		196					No Threat
		195	-5	11	3.456m	Right	Mid
		170				Left	Mid
		165				Left	Mid
		164					No Threat
5	2	360	-7	3	3.456m	Left	High
			5	3	1.99m		
		360	-7	3	3.456m	Right	High
			6	3	1.99m		
		360	-8	3	3.456m	Straight	High
			6	3	1.99m		

7.2 VIRTUAL SENSOR

For the static sensor algorithm validation is trivial. To confirm the dynamic sensors algorithm the code was developed in MATLAB then rewritten in C. The program and source code is included in - Software. The simple executable queries the user to input the number of steps to take and the heading angle then reports back the position in space for each object and the distances for each sensor to the closes object it detects. These values are confirmed against theoretical values. A test environment is defined below and test cases outlined in Table 2.

```c
#define STEP_SIZE 0.5 //meters


/* {X_COOR,Y_COOR} */
float objects[NUM_OBJECTS][2] = {  {0,3},
                                   {3,3},
                                   {-3,3}
                                };
/* {ANG_START,ANG_WIDTH} */
int16 sensorAng[NUM_SENSORS][2]= {  {-50,10},
                                    {40,10},
                                    {-2,4}
                                 };
```

Table 2: Test cases for Virtual Sensor

Test Case	Heading (deg)	Step Increment	Object 1	Object 2	Object 3	Sensor 1 Distance	Sensor 2 Distance	Sensor 3 Distance
1	90	0	[0,3]	[3,3]	[-3,3]	4.243	4.243	3
	90	2	[0,2]	[3,2]	[-3,2]	0	0	2
	90	2	[0,1]	[3,1]	[-3,1]	0	0	1
	90	3	[0,-0.5]	[3,-0.5]	[-3,-0.5]	0	0	0
	270	0	[0,-0.5]	[3,-0.5]	[-3,-0.5]	0	0	0.5
2	45	0	[0,3]	[3,3]	[-3,3]	3	0	4.243
	135	0	[0,3]	[3,3]	[-3,3]	0	3	4.243
	90	6	[0,0]	[3,0]	[-3,0]	0	0	0
	180	1	[0.5,0]	[3.5,0]	[2.5,0]	0	0	2.5
3	45	6	[-2.121,0.879]	[0.879,0.879]	[5.121,0.879]	0	0	1.243
4	135	4	[1.414,1.586]	[4.414,1.586]	[-1.586,1.586]	0	0	2.243

7.3 SYSTEM TESTING

The device was mounted to the left hip of the subject. A 3x4 metre grid was laid out on a carpeted floor using masking tape. The skins on the mastoid processes were lightly cleaned using isopropyl alcohol with no excessive scrubbing. Ten-20 conductive gel was applied to the 1cm diameter gold electrodes which were held in place over the mastoid process using fabric band-aids.

The first tests used the static virtual sensors detailed in section 5.6 The test cases were programmed prior to each test by another person. The subject using the system was unaware of the programmed data. The subject was blindfolded and spun around twice in a circle to calibrate the magnetometer. A metronome was used and the subject attempted to walk at a cadence of 52 steps/min. The two simplest test cases were to use a series of objects all on the left or right side of the subject. The stimulation strength was fixed at 2.5mA.

```
                                /* {ANG_START,ANG_WIDTH} */
static int16 sensorAng[NUM_SENSORS][2]= {   {-15,2},{-10,2},
                                            {-7,2} ,{-4,2},
                                            {-2,2} ,{0,2},
                                            {4,2}  ,{7,2},
                                            {10,2} ,{15,2}

                                        };
/* Test case 1: Objects to Right*/
static float sensorDist[NUM_SENSORS] = { 0,0,0,0,0,
                                         2,2,2,2,2, };
/* Test case 2: Objects to Left*/
static float sensorDist[NUM_SENSORS] = { 2,2,2,2,2,
                                         0,0,0,0,0, };
```

The subjects' movement was recorded using a video camera. LEDS were added to the PIC18F4580 to indicate on the camera when stimulation was turned on and what direction it was in. The videos were analyzed and the subjects feet placement graphed.
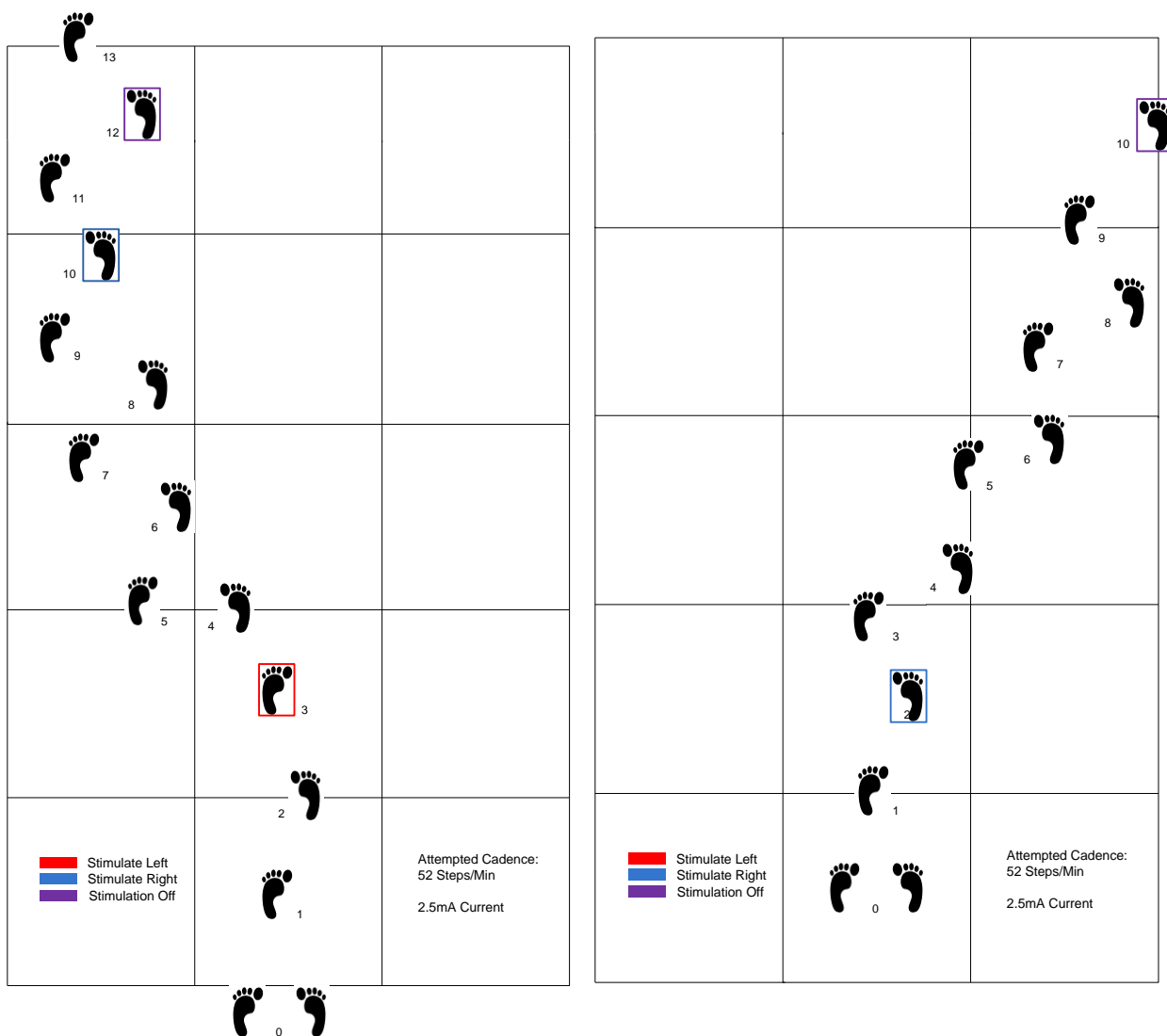
Figure 39: System Testing. Left: Test Case 1, Right: Test Case 2

The magnetometer readings by the PIC18F4580 were already found to fluctuate by about 3 degrees for a fixed sensor position. With the system mounted to a moving person, the size of the breadboard on which the sensor was mounted becomes a large issue in obtaining an accurate heading. The motion of the sensor during walking in conjunction with the fluctuations in sensor readings due to noise results in varying heading readings. Consequently testing of the system using the dynamic sensor wasn't possible. Attempts were made however reproducible results weren't obtainable.

DISCUSSION

8.1 SYSTEM DESIGN

Subsystems with the exception of the magnetometer, performed as expected when tested individually. When testing the entire system certain problems arise and many shortcomings of the design are revealed. Starting with the delivery of the GVS stimulation itself, it's apparent from the measured voltage drop over the electrodes that the power supply used is more than sufficient. For skin treated with alcohol, gold electrodes and conductive gel the measured impedence of the tissue electrode interface was typically less than 10kΩ. This impedance is lower than what was initially expected during literary research and design. In order to deliver a 3mA current pulse to the maximum voltage required by the SMPS is at most 30V. These lower voltages mean less power is required and as such smaller components could be used. Increasing the switching frequency could accommodate smaller inductances and reduce output amount of power. Appropriate PCB design would be required as this switching frequency increases to cut down on switching noise. Using a smaller electrolytic capacitor instead of the large film capacitor should be investigated as well.

Reducing the power of the SMPS should also be considered. Limiting the power to around 300mW means that a maximum current of 7mA can be delivered at 42.5V. This limits the amount of current that could be delivered in case of a component failure hence improving safety of the device. Increasing the switching frequency can be used to reduce power as well as using a 5V regulated input instead of 10V.

In order to protect the current source op-amp and hence the user, the output of the SMPS should have a zener diode added in parallel with the tank capacitor to limit the output voltage in case of regulation failure. Is the desired voltage rails are ±42.5V as implemented in this project, then a 47V zener such as the 1N5261B-T from Diodes Inc. can be used. During regular operation the reverse bias current is in the nano-ampere range which shouldn't affect the performance of the SMPS. Zener breakdown doesn't occur until ±47V which would only be reached if regulation fails. The simulated result of using the zener is shown in Figure 40. Note that the 1N5262 diode (51V zener voltage) was used since the model was readily available. Similar performance is expected with the 1N5261.
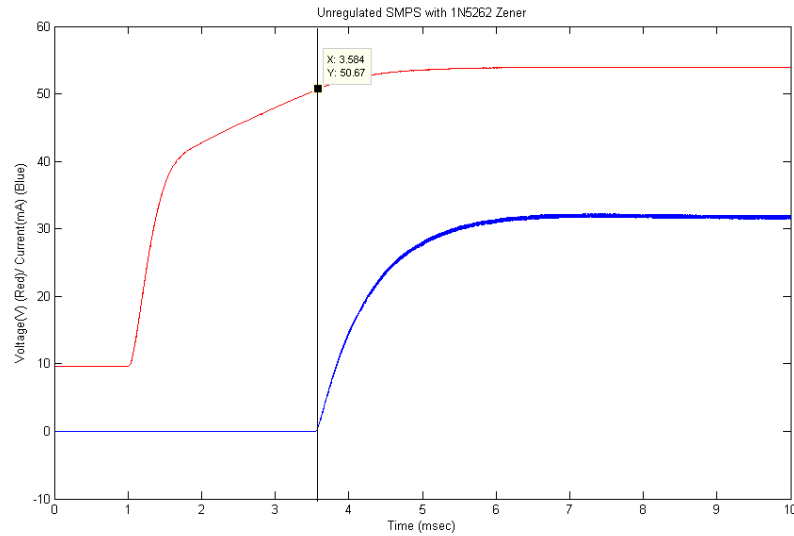
Figure 40: Unregulated SMPS simulation with 1N5262 Zener Diode. Red is output voltage (V), Blue is current (mA) through diode

The PA78 chosen initially for this design is also unnecessary. Cheaper, lower voltage op-amps that can run on supply rails of ±25V could be used. The OPA445 which runs on a maximum of ±45 supply rails, is a suitable choice however cheaper components could be used in order to save cost. Having the additional voltage available though has its advantages as well. If the skin is not treated properly and excess grease, dirt and remnants of the stratum corneum still persist then these higher voltages will still be able to deliver the required currents over the increased impedence.

The tests carried out in this project were short in duration meaning no significant charge build across the tissue due to monophasic pulses have occurred. For prolonged use and stimulation biphasic pulses should examined [26]. Care needs to be taken such that during the charge balance phase of the pulse, the current is less than threshold so as not to induce any stimulation.

The TMU also presented some problems during testing. Mounting the device to the hip of the user induces a lot of motion in both the vertical and horizontal axis. The horizontal motion due to the circuit bouncing off the side of the users' leg causes deviations in the measured heading angle from the HMC1022 magnetometer. As no tilt compensation is used, this fluctuation in the measured heading value causes problems with the Nearness Diagram algorithm. In addition a higher order active filter could be used to limit some noise in the signal. The original intention for adding the HMC1022 was to do course correction after stimulating a

person in a set direction. This was not implemented in the project however due to time constraints and problems in obtaining accurate reliable heading readings. If course correction is to be eventually added then implementing the circuit on a smaller PCB so as to reduce the amount of motion during walking could also fix this problem. Adding a third magnetic sensor axis for tilt compensation could also help remove fluctuations in the measurements.

8.2 SYSTEM PERFORMANCE

One of the goals of this project was to investigate the feasibility of using GVS as a method to direction a person around obstacles in order to avoid collisions. The results from the basic testing done using a static virtual sensor indicate that it is possible. The results indicate the subjects' trajectory was able to be altered from a collision course however the test setup was very simplistic and only really shows basic system functionality. Attempting to implement more complex scenarios to navigate was impeded due to problems with obtaining accurate and reliable readings from the HMC1022.

Since more advanced testing could not be done in the timeframe of this project, properly quantifying the systems performance as a collision avoidance device was not completed.

CONCLUSION

A battery powered modular collision avoidance system implementing galvanic vestibular system was successfully developed in this project. Using simple test cases, the device was shown to be able to redirect a person while walking in order to avoid a collision. Using a CAN network of 8-bit microcontrollers allowed for a modular design independent of the sensors used in the system. Problems were encountered with the magnetometer used which impeded further testing during the timeframe of this project. The systems effectiveness as a collision avoidance system therefore remains unquantified.

Suggested paths for future work should focus on miniaturizing the device and reducing noise. This would improve the devices performance and potentially allow for more complex test scenarios to be carried out. Increasing the safety of the device by limiting the power output of the SMPS and adding zener diodes to deal with any regulation failure should be done. For prolonged

use the device should also move towards a biphasic pulse shape to negate any build up of charge across the stimulated tissue.

REFERENCES

[1] S. Cardin, "A wearable system for mobility improvement of visually impaired people," *The Visual Computer,* vol. 23, pp. 109, 2007.

[2] B. Shin and C. Lim. 2007, Obstacle detection and avoidance system for visually impaired people. Haptic and Audio Interaction Design pp. 78-85. Available: http://dx.doi.org.libaccess.lib.mcmaster.ca/10.1007/978-3-540-76702-2_9

[3] J. Borenstein, "Obstacle avoidance with ultrasonic sensors," *IEEE Journal of Robotics and Automation,* vol. 4, pp. 213, 1988.

[4] A. S. Cauquil, P. Bousquet, M. C. Salon, P. Dupui and P. Bessou. Monaural and binaural galvanic vestibular stimulation in human dynamic balance function. *Gait Posture 6(3),* pp. 210-217. Available: http://resolver.scholarsportal.info/resolve/09666362/v06i0003/210_mabgvsihdbf

[5] L. R. Bent, B. J. McFadyen, V. French Merkley, P. M. Kennedy and J. T. Inglis. Magnitude effects of galvanic vestibular stimulation on the trajectory of human gait. *Neurosci. Lett. 279(3),* pp. 157-160. Available: http://resolver.scholarsportal.info/resolve/03043940/v279i0003/157_meogvsottohg

[6] D. Wardman, J. Taylor and R. Fitzpatrick, "Effects of galvanic vestibular stimulation during human walking," *J. Physiol. (Lond.),* vol. 517, pp. 931, 1999.

[7] J. Minguez, "Nearness diagram navigation (ND): A new real time collision avoidance approach," *IEEE International Conference on Intelligent Robots and Systems,* vol. 3, pp. 2094, 2000.

[8] J. Minguez and L. Montano, "Nearness diagram (ND) navigation: collision avoidance in troublesome scenarios," *Robotics and Automation, IEEE Transactions on,* vol. 20, pp. 45-59,

[9] A. E. Pavlik, J. T. Inglis, M. Lauk, L. Oddsson and J. J. Collins. The effects of stochastic galvanic vestibular stimulation on human postural sway. *Exp. Brain Res. 124(3),* pp. 273-280. Available: http://resolver.scholarsportal.info/resolve/00144819/v124i0003/273_teosgvsohps

[10] N. Nagaya, M. Sugimoto, H. Nii, M. Kitazaki and M. Inami, "Visual perception modulated by galvanic vestibular stimulation," in 2005, pp. 78-84.

[11] M. Bikson, A. Datta and M. Elwassif. 2009. Establishing safety limits for transcranial direct current stimulation. *Clinical Neurophysiology 120(6),* pp. 1033-1034. Available: http://resolver.scholarsportal.info/resolve/13882457/v120i0006/1033_eslftdcs

[12] M. R. Prausnitz. 1996, The effects of electric current applied to skin: A review for transdermal drug delivery. *Adv. Drug Deliv. Rev. 18(3),* pp. 395.

[13] A. Van Boxtel. 1977, Skin resistance during square-wave electrical pulses of 1 to 10 mA. *Medical Biological Engineering Computing 15(6),* pp. 679.

[14] D. T. Lykken.1970, SQUARE-WAVE ANALYSIS OF SKIN IMPEDANCE. Psychophysiology 7(2), pp. 262-275. Available: http://dx.doi.org.libaccess.lib.mcmaster.ca/10.1111/j.1469-8986.1970.tb02232.x

[15] J. Rosell, J. Colominas, P. Riu, R. Pallas-Areny and J. G. Webster. 1988, Skin impedance from 1 hz to 1 MHz. *Biomedical Engineering, IEEE Transactions on 35(8),* pp. 649-651.

[16] W. Besio and A. Prasad. Analysis of skin-electrode impedance using concentric ring electrode. Presented at Engineering in Medicine and Biology Society, 2006. EMBS '06. 28th Annual International Conference of the IEEE.

[17] A. Scinicariello. 2001, Enhancing human balance control with galvanic vestibular stimulation. *Biol. Cybern. 84(6),* pp. 475.

[18] Bosch, CAN specification version 2.0. Published by Robert Bosch BmbH, September 1991

[19] Microchip Technology, Generating High Voltage using the PIC16C781/782, Tech. Bulletin 053. 2005. pp. 1-6.

[20] J. Barrow, Reducing Ground Bounce in DC-to-DC Converters, Analog Dialogue, vol. 41(6) 2007 pp. 1-5.

[21] Natural Resources Canada, Geomagnetism: Magnetic Field Calculator, Available: http://geomag.nrcan.gc.ca/apps/mfcal-eng.php [Accessed: 31/03/2010]

[22] Analog Devices, Using the ADXL202 in Pedometer and Personal Navigation Applications, App. Note 602. 2002. pp. 1-2.

[23] Microchip Technology, PIC18C ECAN 'C' Routines, App. Note 878. 2003

[24] A. Pressman, Switching Power Supply Design. 2nd ed. New York: McGraw-Hill, 1998.

[25] Microchip Technology, "PIC18F2480/2580/4480/4580 " Datasheet, Rev. C March 2007.

[26] E. K. F. Lee and A. Lam. A matching technique for biphasic stimulation pulse. Presented at Circuits and Systems, 2007. ISCAS 2007. IEEE International Symposium on.

APPENDIX A - ACRONYMS

ADC	Analog to Digital Converter
BRP	Baud Rate Prescaler
CAN	Controller Area Network
DAC	Digital to Analog Converter
ECAN	Enhance Controller Area Network
EEG	Electroencephalogram
EMI	Electromagnetic Interference
ESR	Effective Series Resistance
FIFO	First In First Out
FOV	Field of View
GVS	Galvanic Vestibular Stimulation
ICD	Interface Control Document
IDE	Integrated Development Environment
ISR	Interrupt Service Routine
MCU	Master Control Unit
MUX	Multiplexor
ND	Nearness Diagram
PND	Nearness Diagram from the Central Point
PWM	Pulse Width Modulation
RND	Nearness Diagram from the Robot
SMPS	Switching Mode Power Supply
TMU	Trajectory Measurement Unit

APPENDIX B - INTERFACE CONTROL DOCUMENT

See the enclosed document entitled "Interface Control Document: Galvanic Vestibular Stimulation Collision Avoidance System".

APPENDIX C - COMPONENTS LIST

INDEX	QUANTITY	MANUFACTURER	MANU. PART NUM	DIGIKEY PART NUM	DESCRIPTION
1	1	FAIRCHILD SEMICONDUCTOR	FDU3N40	FDU3N40TU-ND	MOSFET N-CH 400V 2A IPAK
2	2	STMICROELECTRONICS	STTH803D	497-7607-5-ND	DIODE SECONDARY 8A 300V TO-220AC
3	2	AVX CORPORATION	FFB24I0755K	478-5361-ND	CAP 7.5UF 400V FILM POWER
4	1	TEXAS INSTRUMENTS	CD74HCT4053E	296-2121-5-ND	IC MUX/DEMUX TRIPLE 2X1 16DIP
5	1	FREESCALE SEMICONDUCTOR	MMA1270EG	MMA1270EG-ND	IC ACCELEROMETER Z AXIS 16-SOIC

6	1	MICROCHIP	PIC18F2480	PIC18F2480-I/SP-ND	IC PIC MCU FLASH 8KX16 28DIP
7	1	HONEYWELL MICROELECTRONICS	HMC1022	342-1005-1-ND	SENSOR LINEAR MAGN 2 AXIS 16SOIC
8	1	ALPHA & OMEGA SEMICONDUCTOR	AOP605	785-1140-5-ND	MOSFET N/P-CH COMPL 30V 8-PDIP
9	2	NATIONAL SEMICONDUCTOR	LM340T	LM340T-5.0-ND	IC REGULATOR POSITIVE 5V TO-220
10	1	STMICROELECTRONICS	L78S10CV	497-6039-5-ND	IC REG POS VOLT 2A 10V TO-220
11	2	MURATA POWER SOLUTIONS	33221C	811-1234-ND	INDUCTOR 220UH 1.6A T/H TOROID
12	1	VISHAY IR	IRFU9310PBF	IRFU9310PBF-ND	MOSFET P-CH 400V 1.8A I-PAK
13	A/R[1]	VISHAY/DALE	N/A	CMF10.0KHFCT-ND	RES 10.0K OHM 1% 50PPM 1/2W
14	A/R	VISHAY/DALE	N/A	CMF100KHFCT-ND	RES 100K OHM 1% 50PPM 1/2W
15	A/R	VISHAY/DALE	N/A	CMF1.00KHFCT-ND	RES 1.00K OHM 1% 50PPM 1/2W
16	A/R	N/A	N/A	N/A	RES 100 OHM 1W 1%
17	1	MURATA ELECTRONICS	PV37W502C01B00	490-2983-ND	TRIMPOT CERM 5K OHM 12TRN TOP
18	A/R	VISHAY/BC	N/A	1109PHCT-ND	CAP 50V .1UF AXIAL CERAMIC X7R
19	A/R	VISHAY/BC	N/A	1001PHCT-ND	CAP 50V 100PF AXIAL CERAMIC C0G
20	A/R	TDK CORPORATION	N/A	445-2857-ND	CAP CER 1UF 25V X7R RAD
21	A/R	TDK CORPORATION	N/A	445-4820-ND	CAP CER 10UF 16V Y5V RAD
22	1	MICROCHIP	TC4228CPA	TC4428CPA-ND	IC MOSFET DVR 1.5A DUAL HS 8-DIP
23	A/R	PANASONIC	N/A	P824-ND	1.0UF 50V MINI ALUM ELECT (KA)
24	1	MICROCHIP	PIC18F1230	PIC18F1230-E/P-ND	IC PIC MCU FLASH 2KX16 18DIP
25	3	ECS INC	ECS-100-S-1X	X992-ND	CRYSTAL 10.000 MHZ SER 49UA
26	A/R	VISHAY B/C	N/A	BC1003CT-ND	CAP 15PF 50V CERAMIC C0G 5%
27	A/R	LITE-ON	LTL-4223	160-1127-ND	LED 5MM HI-EFF RED DIFFUSED
28	A/R	KEMET	N/A	399-4261-ND	CAP .01UF 200V 10% CER RADIAL
29	A/R	KEMET	N/A	399-4145-ND	CAP 1000PF 200V 10% CER RADIAL
30	A/R	KEMET	N/A	399-4290-ND	CAP 33PF 200V 5% CER RADIAL
31	A/R	VISHAY/BC	N/A	BC1114CT-ND	CAP .10UF 100V CERAMIC X7R 10%
32	A/R	PANASONIC	N/A	P120CACT-ND	RES METAL FILM 120 OHM 1/4W 1%
33	1	MICROCHIP	PIC18F4580	PIC18F4580-I/P-ND	IC PIC MCU FLASH 16KX16 40DIP
34	2	TEXAS INSTRUMENTS	TLV2375	296-12222-5-ND	IC OPAMP GP R-R 3MHZ QUAD 16DIP
35	1	MICROCHIP	MCP6042	MCP6042-I/P-ND	IC OPAMP 1.4V DUAL SGL SPLY 8DIP
36	1	TEXAS INSTRUMENTS	OPA445	OPA445AP-ND	IC OPAMP GP 2MHZ SGL HV 8DIP
37	1	CIRRUS LOGIC	PA78EU	598-1440-ND	IC PWR AMP 350V 200MA 12SIP
38	A/R	N/A	N/A	N/A	RES 1MOHM 1W 1%
39	2	MICROCHIP	MCP2551	MCP2551-I/P-ND	IC TRANSCEIVER CAN HI-SPD 8-DIP
40	2	MICROCHIP	TC962	TC962CPA-ND	IC CHARGE PUMP DC/DC CONV 8-DIP
41	2	TEXAS INSTRUMENTS	INA128P	INA128P-ND	IC OPAMP INSTR 1.3MHZ SGL 8DIP
42	2	N/A	N/A	N/A	1CM DIAM GOLD ELECTRODE EEG

[1] A/R Indicates to use as many as required by schematic

APPENDIX D - SOFTWARE

Software used in the implementation of this system is enclosed on a DVD. 'MCUMain' is the software developed for the PIC18F4580 which acts as the MCU. 'SMPS' is the software for the PIC18F1230 which controls the SMPS. 'ECAN' contains the software included in Application Note 878 [23] with the definitions required for building it. 'VirtualSensor' contains the software used on the PIC18F2480 to simulate a series of sensor nodes in the system. All software was written for the Microchip C18 tool suite and developed in the MPLAB IDE.

APPENDIX E - SCHEMATICS

Although all schematics are included in this report however their original soft copies designed in Cadence OrCad Capture v16 are in the enclosed DVD under the folder 'Schematics'.

Vitae

NAME:	PAUL T. QUEVEDO
PLACE OF BIRTH:	BRAMPTON, ONTARIO
YEAR OF BIRTH:	1986
SECONDARY EDUCATION:	ST. THOMAS AQUINAS SECONDARY SCHOOL (2000-2004)
HONOURS AND AWARDS	

- MCMASTER ENTRANCE SCHOLARSHIP
- MCMASTER UNDERGRADUATE RESEARCH PROGRAM (2006-2007)
- NSERC USRA (2007)
- DEANS HONOUR LIST (2006-2009)